ANALYSIS OF PHOTONIC NANOJETS FORMED BY A FOCUSED INCIDENT BEAM USING VECTOR SPHERICAL HARMONICS EXPANSION

A Thesis

by

AOTUO DONG

Submitted to the Office of Graduate and Professional Studies of
Texas A&M University
in partial fulfillment of the requirements for the degree of

MASTER OF SCIENCE

Chair of Committee,	Chin B. Su
Committee Members,	Philip R. Hemmer
	Jim Ji
	Sy-Bor Wen
Head of Department,	Jose Silva-Martinez

May 2015

Major Subject: Electrical Engineering

ABSTRACT

The analysis of photonic nanojets formed by dielectric spheres generally assumes that the incident field is a plane wave. In this work, using vector spherical harmonics representations, we analyze the case of a more realistic incident field consisting of a focused beam formed by microscope objectives with low as well as high numerical aperture. The nanojet solution is exact with practical number of spherical harmonic terms. In contrast with a plane wave analysis, we are able to include in the analysis cases in which the sphere is at the focal plane of the focus beam and away from the focal plane. We found that the nanojet beam waist dimension is less sensitive with respect to the azimuthal angle when compare with the plane wave case. Also, by shifting the particle away from the focal plane, the nanojet beam waist can be positioned outside the particle which otherwise would be inside or at the particle surface. Different relative positions of the particle and the focused beam along the propagating axis are discussed as well as different particle size. The bwam waist can achieve 130 nm when the diameter of the particle is 2 um. The results are compared with the plane wave case.

ACKNOWLEDGMENTS

This dissertation would not have been possible without the support of my advisor for scholarly advice and guidance.

I would like to thank my parents who support me until graduate.

I also thank my friends who encourage me to finish this research.

TABLE OF CONTENTS

Page

LIST OF FIGURES

Page

LIST OF TABLES

Page

1. INTRODUCTION*

1.1 Literature Review

2-D photonic nanojet formed by a dielectric cylinder [1] and the sensitivity of its backscattered light to the presence of small particles was first reported in 2004 using FDTD analysis [1]. Using vector spherical harmonic function, 3-D nanojets formed by various particle size and index were calculated as well as their sensitivity of backscattered light perturbed by nanoparticles [2]. Field distribution of nanoparticles on Si surface was studied [3]. These topics and potential applications of nanojets were reviewed in [4]. An application was the used of an array of micro-particles to create an array of blind holes in Si [5]. Another interesting application related to the sub-wavelength capability of nanojets formed by micro-particles is the super-resolution imaging capability of these micro-particles [6]. A host of other articles on the detail analysis and presentations of nanojets can be found in [7-12]. Photonic nanojets were indirectly observed from measurements of two-photon fluorescence enhancement of molecules within a solution with silica microspheres [13], and also in triangular photonic molecules [14]. It was directly measured by data deconvolution on 3-D maps of light passing through the confocal pinhole of a confocal microscope system [15]. Sensitivity of backscattered light to perturbation from small nanoparticles in front of the nanojet has

* Parts of the thesis are reprinted with permission from "Analysis of a Photonic Nanojet Assuming a Focused Incident Beam Instead of a Plane Wave" by Aotuo Dong and Chin Su, 2014. *Journal of Optics*, 16(12), Copyright [2014] by IOP.

also been measured [16]. Nanojets were also formed by thin planar disks with diameter of 1-10 um [17], and on chains of coupled spherical cavities [18].

1.2 Statement of the Problem

The analysis of nanojets generally assumes that the incident field is a plane wave. In this work, we investigate the nanojet formed by a focused incident beam with a spot size smaller or comparable to the particle size. We find that the usage of the vector spherical harmonics expansion of the focused beam allows a rigorous calculation of the 3-D nanojets for the case when the particle center is at or away from the focal point. Not surprisingly we find that the position of the nanojet beam waist with respect to the particle surface can be adjusted by moving the particle's position about the focal point with little change in the nanojet dimension. It is also found that the nanojet spot size is more symmetric with respect to the azimuthal angle than the case if the incident field is a plane wave. In reference 19, vector spherical harmonics were first used in the expansion of an incident convergent beam incident on a spherical microparticle the size of λ. However, the reported focal spot formed is inside the particle in order to mimic the focal spot formed by a hemispherical lens.

1.3 Method of Procedure

We find that the usage of the vector spherical harmonics expansion of the focused beam allows a rigorous calculation of the 3-D nanojets for the case when the particle center is at or away from the focal point. The incident field E_i is expanded in terms of the orthogonal vector spherical harmonics. The full expression for the vector spherical harmonics M_{emn}, M_{omn}, A_{emn}, and A_{omn} as a function of spherical coordinates (r_p, θ_p, ϕ_p) are listed in ref [25] equation 4-17-20

Contrast to reference [2, 19, 25], we provide an additional integration with respect to r_p. To describe the field E_i at any point (r_p, θ_p, ϕ_p) in the image space of a microscope objective. Denote the scattered electric and magnetic fields outside the particle as E_a and H_a. Inside the particle fields are denoted as E_b and H_b. When r_p is outside the particle, the total field consists of the incident field plus the scattered field. Tangential components of the electric and magnetic fields in the e_θ and e_ϕ direction must be equal at the particle-medium interface at $r_p = r_b$.

E_i consists of a linear combination of M_{o1n} and N_{e1n}, therefore based on (A14) E_a and E_b are also a linear combination of M_{o1n} and N_{e1n}. With α_{an}, α_{bn}, β_{an}, β_{bn} calculated and E_n obtained from (A16) for the case of the focused beam, all electric and magnetic fields as a function of (r_p, θ_p, ϕ_p) are given. The nanoshell has the similar procedure to this one but it needs more equations between the gold shell and the dielectric core.

2. OPTICAL CONFIGURATIONS AND CALCULATION PARAMETERS

2.1 Case One

Figure 1 depicts the optical configuration and parameters used in this analysis.

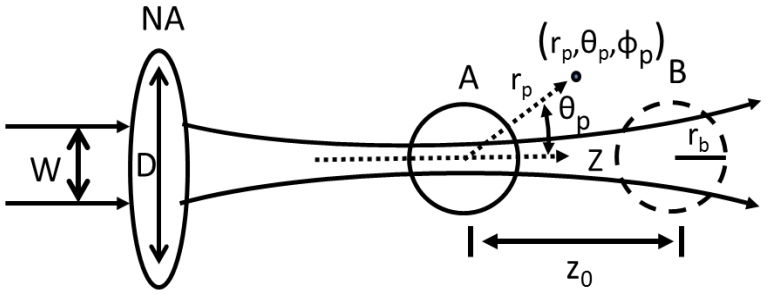

Figure 1. Optical configuration and parameters used in this analysis

A collimated x-polarized Gaussian input beam with beam width W impinges on a microscope objective with a numerical aperture denoted by NA. The aperture at the back focal plane of the microscope objective is D. Any point in the image plane of the microscope objective is denoted in spherical coordinates as (r_p, θ_p, ϕ_p). The analysis is made for the particle at position A at the focal point and at position B away from the focal point as shown. For this analysis, the collimated beam diameter is fixed at W=2 mm and D= 7.65 mm. NA=0.4 or 0.8. The particle diameter is fixed at 2 um, and its refractive index is taken as 1.47. The wavelength is 400 nm.

Another depiction of the optical configuration with some useful parameters is given below.

2.2 Case Two

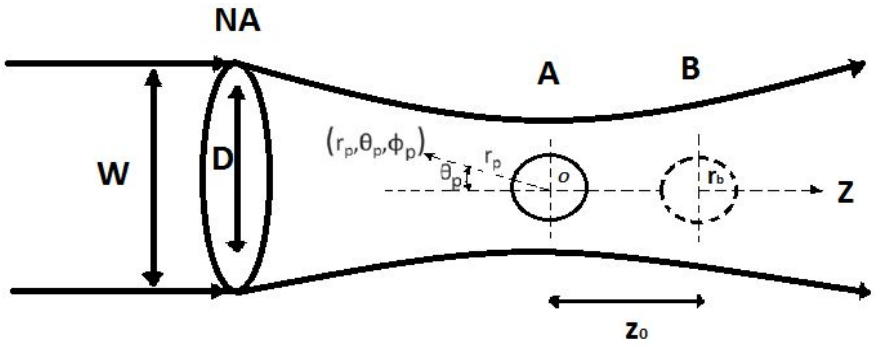

Figure 2. Another optical configuration and parameters used in this analysis

An x-polarized Gaussian beam with a width of W impinging on a microscope objective with a numerical aperture of 0.9 which can make the best focus effect in practice. We also decide the incident impinging beam occupying the total aperture, say, W=D=7.65um, because this way will make the focused beam big enough to hold the particles like A and B while maintaining the property of Gaussian beam undoubtedly. The particle diameter could be changed related to the beam waist in terms of each local position along Z direction. The refractive index of the particle is 1.47 while the wavelength of the beam is 400 nm.

2.3 Case Three

In this case, the particle could be replaced by a nanoshell covered with gold metal from the two cased above, and the parameters of the beam could be changed as well.

3. IMAGE PLANE FORMULA

The expressions for the vector field $E(x, y, z)$ in the image region of the lens may be derived by an application of the formula given below [20],

$$\mathrm{E(x, y, z)} = -\frac{ik}{2\pi}\iint_{\Omega}\frac{a(s_x, s_y)}{s_z}e^{ik[\Phi(s_x,s_y)+s_x x+s_y y+s_z z]}ds_x ds_y \tag{1}$$

Where (x, y, z) is any point in the image space, and (s_x, s_y, s_z) represents the unit vector at various points at the exit pupil to (x, y, z). The incident field strength at the exit pupil is described by $a(s_x, s_y)$. According to Richards and Wolf [20], using the formula given above, the following expressions are obtained for the Cartesian components of the field vectors at point $P = (x, y, z)$.

$$E(P) = E_x(P)\cdot\hat{e}_x + E_y(P)\cdot\hat{e}_y + E_z(P)\cdot\hat{e}_z$$

$$E_x(P) = -i\pi\cdot(I_0 + I_2\cos 2\phi_P)$$

$$E_y(P) = -\pi\cdot I_2\sin 2\phi_P$$

$$E_z(P) = 2i\pi\cdot I_1\cos\phi_P \tag{2}$$

By using the transformation formula given below, we transformed the E field in Cartesian coordinate into spherical coordinates which is more appropriate for analysis of scattering off spherical particles.

$$\hat{e}_x = \sin\theta_P\cos\phi_P\hat{e}_r + \cos\theta_P\cos\phi_P\hat{e}_\theta - \sin\phi_P\hat{e}_\phi$$

$$\hat{e}_y = \sin\theta_P\sin\phi_P\hat{e}_r + \cos\theta_P\sin\phi_P\hat{e}_\theta + \cos\phi_P\hat{e}_\phi$$

$$\hat{e}_z = \cos\theta_P\hat{e}_r - \sin\theta_P\hat{e}_\theta \tag{3}$$

The x-polarized electric field $E_i(r_p,\theta_p,\phi_p)$ at any point in the image space if expressed in spherical coordinate is:

$$E_i(r_p,\theta_p,\phi_p) = E_r \cdot \hat{e}_r + E_\theta \cdot \hat{e}_\theta + E_\phi \cdot \hat{e}_\phi$$

$$\begin{aligned} E_r &= -\pi \cos\phi_p \cdot [I_0(r_p,\theta_p) + I_2(r_p,\theta_p)] \cdot \sin\theta_p - 2iI_1(r_p,\theta_p)\cos\theta_p \\ E_\theta &= -\pi \cos\phi_p \cdot [I_0(r_p,\theta_p) + I_2(r_p,\theta_p)] \cdot \cos\theta_p + 2iI_1(r_p,\theta_p)\sin\theta_p \\ E_\phi &= \pi \sin\phi_p \cdot [I_0(r_p,\theta_p) - I_2(r_p,\theta_p)] \end{aligned} \quad (4)$$

Where I_0 , I_1 and I_2 are given by,

$$\begin{aligned} I_0(r_p,\theta_p) &= \int_0^\alpha \sqrt{\cos\theta}\,\sin\theta(1+\cos\theta)J_0(k_a r_p \sin\theta\sin\theta_p)\exp(ik_a r_p \cos\theta\cos\theta_p F(\theta)d\theta \\ I_1(r_p,\theta_p) &= \int_0^\alpha \sqrt{\cos\theta}\,\sin^2\theta \cdot J_1(k_a r_p \sin\theta\sin\theta_p)\exp(ik_a r_p \cos\theta\cos\theta_p F(\theta)d\theta \\ I_2(r_p,\theta_p) &= \int_0^\alpha \sqrt{\cos\theta}\,\sin\theta(1-\cos\theta)J_2(k_a r_p \sin\theta\sin\theta_p)\exp(ik_a r_p \cos\theta\cos\theta_p F(\theta)d\theta \end{aligned} \quad (5)$$

J_0, J_1, J_2 are Bessel functions and k_a is the medium wavenumber. θ is integrated to α, where $\alpha = \sin^{-1}(NA)$. $F(\theta)$ is the focusing function that we have added to the original formula to describe a collimated input Gaussian beam.

The focusing function $F(\theta)$ is given by [21],

$$F(\theta) = \exp\{-0.5 \cdot \ln(2) \cdot (\frac{D}{W \cdot NA})^2 \cdot \sin^2(\theta)\} \quad (6)$$

Where D is the diameter of the back focal aperture of the objective and W is the FWHM of the collimated incoming Gaussian beam (see figure 1). (6) is not normalized with respect to the incident optical power, which is not an issue for calculations presented here.

The expression for I_0 , I_1 and I_2 given above is to be used when the focal spot coincide with the center of the particle. If the center of the particle is to be displaced from the center of the focal spot by R, then simple change $r_p \cos\theta_p$ to $r_p \cos\theta_p + R$, with the origin at the particle's center. If R is positive, then the center of the particle at $r_p = 0$ is to the right of the focal plane, which means that the beam is expanding at the particle's coordinate. If R is negative, the opposite is true.

It is noted in another presentation of the focused beam that under paraxial conditions the focusing beam in the image space can be written as a series expansion with respect to the ratio of the beam waist versus diffraction length [22]. If only the first order term is retained then the focusing beam is Gaussian in shape. This Gaussian shape focusing beam at the particle position was used in reference [23] for calculating the nanojet formed by a dielectric particle. The paraxial condition implies that the calculation is valid only if the focus spot is formed by a small numerical aperture objective. We use the Richard and Wolf formula [20] to describe the focusing beam. The input collimated beam before the microscope object is Gaussian, but the image field vector as describe by equations 1 and 2 in the focal region where the particle is located is not, in contrast with reference 23. Furthermore, the Richard and Wolf formula is valid even for numerical aperture approaching one [24]. Furthermore the Richard and Wolf formula is a result of a full vector analysis. Using a microscope objective with NA =0.85, the spatial profile of the focal spot predicted by the Richard and Wolf formula agreed very well with experimentally measured profile using a scanning NSOM probe [21].

4. VECTOR SPHERICAL HARMONICS ANALYSIS

4.1 Incident Beam

The incident field E_i is expanded in terms of the orthogonal vector spherical harmonics as follows,

$$E_i = \sum_{m=0}^{\infty} \sum_{n=m}^{\infty} (B_{emn} \cdot M_{emn} + B_{omn} \cdot M_{omn} + A_{emn} \cdot N_{emn} + A_{omn} \cdot N_{omn}) \tag{7}$$

The full expression for the vector spherical harmonics M_{emn} , M_{omn} , A_{emn} , and A_{omn} as a function of spherical coordinates (r_p, θ_p, ϕ_p) are listed in ref [25] equation 4-17-20:

$$M_{emn} = -\sin m\phi_p \cdot \frac{mP_n^m}{\sin\theta_p} \cdot z_n(\rho) \cdot \hat{e}_\theta - \cos m\phi_p \cdot \frac{dP_n^m}{d\theta_p} \cdot z_n(\rho) \cdot \hat{e}_\phi$$

$$M_{omn} = \cos m\phi_p \cdot \frac{mP_n^m}{\sin\theta_p} \cdot z_n(\rho) \cdot \hat{e}_\theta - \sin m\phi_p \cdot \frac{dP_n^m}{d\theta_p} \cdot z_n(\rho) \cdot \hat{e}_\phi$$

$$N_{emn} = \cos m\phi_p n(n+1) \cdot P_n^m \frac{z_n(\rho)}{\rho} \cdot \hat{e}_r + \cos m\phi_p \cdot \frac{dP_n^m}{d\theta_p} Z_n(\rho) \cdot \hat{e}_\theta - \sin m\phi_p \frac{mP_n^m}{\sin\theta_p} Z_n(\rho) \cdot \hat{e}_\phi$$

$$N_{omn} = \sin m\phi_p n(n+1) P_n^m \frac{z_n(\rho)}{\rho} \cdot \hat{e}_r + \sin m\phi_p \frac{dP_n^m}{d\theta_p} Z_n(\rho) \cdot \hat{e}_\theta + \cos m\phi_p \frac{mP_n^m}{\sin\theta_p} Z_n(\rho) \cdot \hat{e}_\phi$$

$$Z_n(\rho) \equiv \frac{1}{\rho} \cdot \frac{d}{d\rho}[\rho \cdot z_n(\rho)] \tag{8}$$

$P_n^m(\theta_p)$ is the associate Legendre function The radial function $z_n(\rho)$ is either the spherical Bessel function or the Hankel function. $\rho = kr_p$, where k is the wave number. The orthogonal property between the vector spherical harmonics allows the coefficients B_{emn} , B_{omn} , A_{emn} and A_{omn} to be written as,

$$B_{emn}=\frac{\int_0^{\infty}\int_0^{2\pi}\int_0^{\pi}E_i\left(r_p,\theta_p,\phi_p\right)\cdot M_{emn}\left(r_p,\theta_p,\phi_p\right)\cdot\sin\left(\theta_p\right)\cdot d\theta_p\cdot d\phi_p\cdot dr_p}{\int_0^{\infty}\int_0^{2\pi}\int_0^{\pi}\left|M_{emn}\left(r_p,\theta_p,\phi_p\right)\right|^2\cdot\sin\left(\theta_p\right)\cdot d\theta_p\cdot d\phi_p\cdot dr_p}$$

$$B_{omn}=\frac{\int_0^{\infty}\int_0^{2\pi}\int_0^{\pi}E_i(r_p,\theta_p,\phi_p)\cdot M_{omn}(r_p,\theta_p,\phi_p)\cdot\sin(\theta_p)\cdot d\theta_p\cdot d\phi_p\cdot dr_p}{\int_0^{\infty}\int_0^{2\pi}\int_0^{\pi}\cdot\left|M_{omn}(r_p,\theta_p,\phi_p)\right|^2\cdot\sin(\theta_p)\cdot d\theta_p\cdot d\phi_p\cdot dr_p}$$

$$A_{emn}=\frac{\int_0^{\infty}\int_0^{2\pi}\int_0^{\pi}E_i\left(r_p,\theta_p,\phi_p\right)\cdot N_{emn}\left(r_p,\theta_p,\phi_p\right)\cdot\sin\left(\theta_p\right)\cdot d\theta_p\cdot d\phi_p\cdot dr_p}{\int_0^{\infty}\int_0^{2\pi}\int_0^{\pi}\left|N_{emn}\left(r_p,\theta_p,\phi_p\right)\right|^2\cdot\sin\left(\theta_p\right)\cdot d\theta_p\cdot d\phi_p\cdot dr_p}$$

$$A_{omn}=\frac{\int_0^{\infty}\int_0^{2\pi}\int_0^{\pi}E_i\left(r_p,\theta_p,\phi_p\right)\cdot N_{omn}\left(r_p,\theta_p,\phi_p\right)\cdot\sin\left(\theta_p\right)\cdot d\theta_p\cdot d\phi_p\cdot dr_p}{\int_0^{\infty}\int_0^{2\pi}\int_0^{\pi}\left|N_{omn}\left(r_p,\theta_p,\phi_p\right)\right|^2\cdot\sin\left(\theta_p\right)\cdot d\theta_p\cdot d\phi_p\cdot dr_p} \tag{9}$$

Note that the ϕ_p dependence of all four vector harmonics in (8) contains either $\sin(\phi_p)$ or $\cos(\phi_p)$ terms, whereas the ϕ_p dependence of E_r, E_θ, E_ϕ. (4) contains only $\sin(\phi_p)$ or $\cos(\phi_p)$. Therefore, all expansion coefficients obtained from equation (6) will be zero unless m=1 since all coefficients are the product of vector harmonics and the incident focused field E_i. And ϕ_p is integrated from 0 to 2 π. Moreover, with $m=1$, coefficients B_{e1n} involving M_{e1n} and A_{o1n} involving N_{o1n} are zero because the integration over ϕ_p involving these terms are always the product of $\sin(\phi_p)$ and $\cos(\phi_p)$ which yields zero. B_{o1n} and A_{e1n} are calculated using equation (A12) which shows that $A_{e1n}=-i\cdot B_{o1n}$. Thus, the only non-zero coefficients in the expansion of E_i are B_{o1n} and A_{e1n} involving M_{o1n} and N_{e1n} respectively. We write E_i' as,

$$E_i'(r_p,\theta_p,\phi_p) = \sum_{n=1}^{\infty} E_n (M_{o1n}^{(0)} - i \cdot N_{e1n}^{(0)}) \tag{10}$$

The superscripts (0) in the vector harmonics indicates that its radial components $z_n(\rho)$ are given by the spherical Bessel functions of the first kind $j_n(k_a r)$, where k_a is the medium wavenumber. Expressions for the spherical vector harmonics M_{o1n} and N_{e1n} for the case $m=1$, after conversion from the Associated Legendre function P_n^1 to the Legendre function P_n, are given in the appendix.

The coefficient $E_n = B_{o1n}$. Note that the form for the incident field E_i' is exactly like the plane wave case except that coefficients which need to be calculated from (A12) are different.

It is necessary to determine the minimum number of summation terms needed in equation (10) so that E_i' can faithfully recreates the expression for the exact incident field E_i given by equation (3). For instance, the value of E_n is calculated using (A12) for a microscope objective with NA = 0.4 for medium focusing power, and 0.8 for strong focusing power. The collimated beam size is fixed at W=2 mm, and objective's back focal plane aperture is fixed at D=7.65 mm. Values of E_n that show the number of summation terms needed are given in Table 1 in the Appendix. For the case of a plane wave, it is well known that $E_n = E_0 \cdot i^n \cdot \dfrac{2n+1}{n(n+1)}$.

Figure 2(a') and (a) show the plot of $\left| E_i'(r_p,\theta_p,\phi_p) \right|^2$ and $\left| E_i(r_p,\theta_p,\phi_p) \right|^2$ versus r_p perpendicular to the optical axis ($\theta_p = \pi/2$) and along the optical axis ($\theta_p = 0$)

using the vector harmonics expansion of equation (7) and the Richard and Wolf formula of equation (4) respectively. The numerical aperture NA=0.4. Figure 2(b') and (b) compare the same plot for NA=0.8. If a sufficient number of summation terms is used, plots using equation (10) or equation (4) are indistinguishable as shown in figure 3, indicating that the vector harmonics expansion is a valid representation of the incident field.

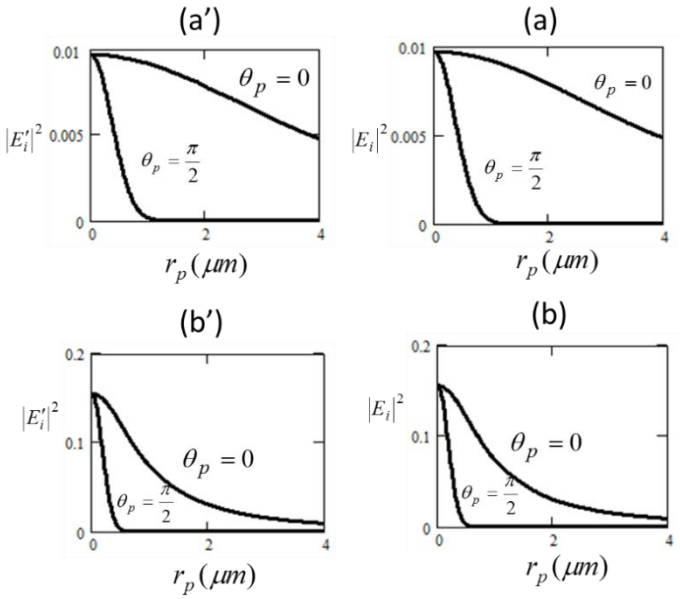

Figure 3. The The comparison of the field intensity for different NA and phases

For the case of the particle displaced from the focal plane by 3.9 um, calculated coefficients E_n and the number of terms needed for both NA=0.4 and 0.8 are also given in Table 1 in the Appendix. For NA=0.4, figure 4(a') and (a) show the plot of $\left| E_i'(r_p, \theta_p, \phi_p) \right|^2$ and $\left| E_i(r_p, \theta_p, \phi_p) \right|^2$ versus r_p for $\theta_p = \frac{\pi}{2}$ and $\theta_p = \pi$ using the vector

harmonic expansion and the Richard and Wolf formula respectively. The coordinate origin at $r_p = 0$ is at the particle's center which is 3.9 um away from the focal point. The FWHM of the beam spot size at the particle position is now 1.2 um as indicated by the case corresponding to $\theta_p = \frac{\pi}{2}$ instead of 0.84 um at the focal point. For the case corresponding to $\theta_p = \pi$, the field intensity peaks at $r_p = 3.9$ um which is the focal point. Figure 4(b') and (b) show the same comparison plot for NA=0.8. The field intensity at the coordinate origin at $r_p = 0$, which is the position of the displaced particle center, is small because of the highly divergent beam for $NA = 0.8$. An expanded view of the field intensity for the case corresponding to $\theta_p = \frac{\pi}{2}$ shows the beam spot size at the particle position is 1.65 um.

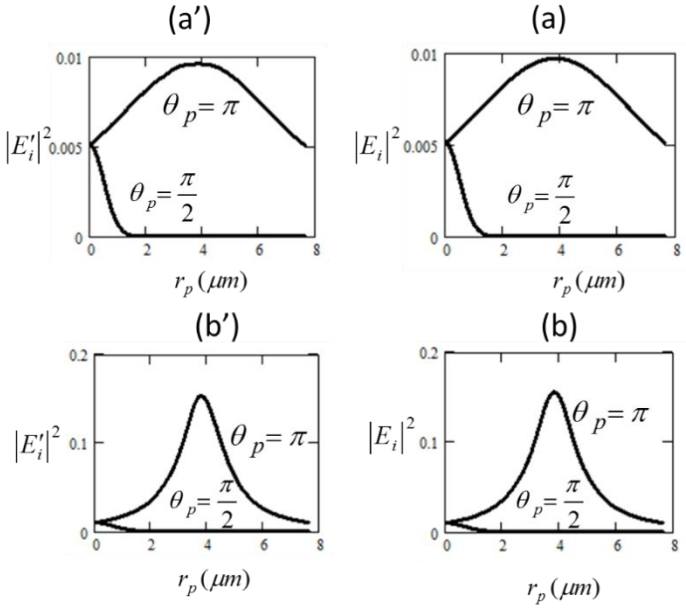

Figure 4. The comparison of the field intensity for different NA and phases when the particle is shifted away from the focused point.

Figure 5 displayed below describes the case when the numerical aperture NA = 0.9. The wavelength is 400 nm. Figure (5a) and (5a') is the case when the origin is at the focal point. Figure (5a) shows show the plot of $\left| E_i'(r_p,\theta_p,\phi_p) \right|^2$ versus r_p perpendicular to the optical axis ($\theta_p = \frac{\pi}{2}$) and two directions along the optical axis ($\theta_p = 0$ and $\theta_p = \pi$) using the vector harmonics expansion of equation (4). Figure (5a') shows the plot using the Richard and Wolf formula of equation (1). Observably, the plots for the two directions along the axis overlapped due to the symmetry about the focal point. The focal spot size is 222 nm which is exactly the same as the result as given by the diffraction limit formula: $\frac{\lambda}{2NA}$. Figure (b) and (b') show the plot of $\left| E_i'(r_p,\theta_p,\phi_p) \right|^2$ when the origin at $r_p = 0$ is at the particle's center which is 191 nm behind forward and in front of the focal point. The FWHM of the beam spot size at both particle positions is 258 nm due to the symmetric property of the focused beam about the focal point. (c) and (c') are generated using the same method but they are 318 nm behind and in front of the focal point, the FWHM of which is 263 nm. As the result generated shows, the symmetric positions about the focal point definitely give us the same shape of the curves.

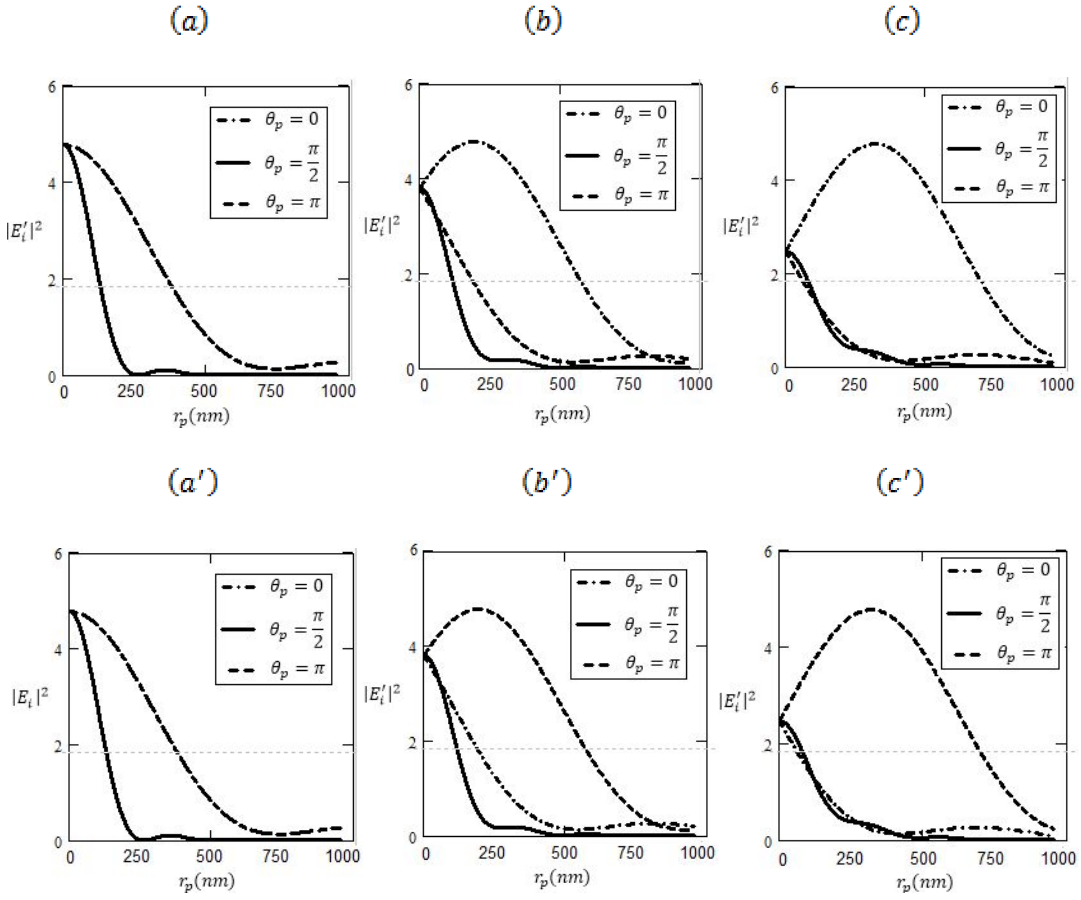

Figure 5. The comparison of the field intensity for another NA when the particle is in different positions

4.2 Nanopaticle Case

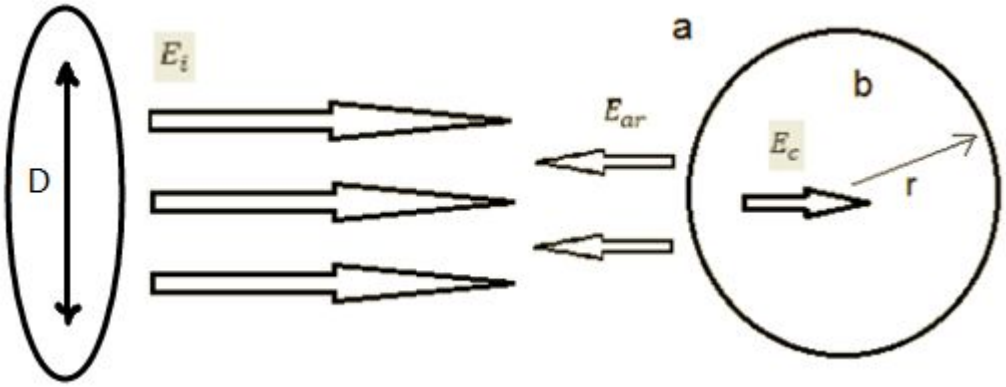

Figure 6. The schematic of beam incident on the nanoparticle

With the validity of the spherical harmonic expansion for the incident field established, we calculate the scattered field off the particle and the field inside the particle. The scattered field is denoted as E_{ar} and the field inside the particle is denoted as E_b , with the same subscript notation for the magnetic field. since the scattered field resembles an outgoing wave, the appropriate general expression for the radial component $z_n(\rho)$ in the spherical harmonic function M and N describing the scattered field is the spherical Hankel function of the first kind: $z_n(\rho) = h_n^{(1)}(k_b r)$, with $h_n^{(1)}(\rho) \equiv j_n(\rho) + i \cdot y_n(\rho)$, where $y_n(\rho)$ is the spherical Bessel function of the second kind E_i. Thus E_{ar}, in vector spherical E_b harmonics, would contain the Hankel function $h_n^{(1)}(\rho)$ representing the outgoing wave. E_b would contain the Bessel function $j_n(\rho)$ like E_i since $h_n^{(1)}(\rho)$ diverges at $\rho = 0$.

Expansion of incident electric field in spherical vector harmonics is given below,

$$E_i = \sum_{n=1}^{\infty} E_n (M_{o1n}^{(0)} - i \cdot N_{e1n}^{(0)}) \tag{11}$$

Since the magnetic wave

$$H_i = \frac{1}{i\omega\mu_a} \nabla \times E_i = \frac{1}{i\omega\mu_a} \sum_{n=1}^{\infty} E_n (\nabla \times M_{o1n}^{(0)} - i \cdot \nabla \times N_{e1n}^{(0)}) \tag{12}$$

We use

$$\nabla \times N = k \cdot M$$

$$\nabla \times M = k \cdot N \tag{13}$$

With

$$k^2 = i\omega\mu \cdot (\sigma - i\omega\varepsilon) \tag{14}$$

While $\sigma = 0$, We get

$$H_i = -\frac{k_a}{\omega\mu_a} \sum_{n=1}^{\infty} E_n (M_{e1n}^{(0)} + i \cdot N_{o1n}^{(0)}) \tag{15}$$

Also, the scattered electric and magnetic wave by the particle surface are

$$E_{ar} = \sum_{n=1}^{\infty} E_n (i \cdot \alpha_{an} N_{e1n}^{(1)} - \beta_{an} M_{o1n}^{(1)})$$

$$H_{ar} = \frac{k_a}{\omega\mu_a} \sum_{n=1}^{\infty} E_n (i \cdot \beta_{an} N_{o1n}^{(1)} + \alpha_{an} M_{e1n}^{(1)}) \tag{16}$$

Where (0), (1) means the use of Bessel function and Hankel function respectively. Inside the particle region, we have

$$E_b = \sum_{n=1}^{\infty} E_n (\beta_{bn} M_{o1n}^{(0)} - i \cdot \alpha_{bn} N_{e1n}^{(0)})$$

$$H_b = -\frac{k_b}{\omega\mu_b}\sum_{n=1}^{\infty} E_n(i\cdot\beta_{bn}N_{o1n}^{(0)} + \alpha_{bn}M_{e1n}^{(0)}) \tag{17}$$

Thus we have four constants to be determined: α_{an}, β_{an}, α_{bn}, β_{bn}. According to formula (8), if the subscript is (0), replace $z_n(\rho)$ into $j_n(\rho)$; if the subscript is (1), replace $z_n(\rho)$ by $h_n^{(1)}(\rho)$. For the interface of a, b, the tangential components of the electric and magnetic fields in the e_θ and e_ϕ direction must be equal at the particle-medium interface. This equality condition on E and H are expressed as:

$$\begin{aligned}(E_i + E_a)_{\theta,\phi} &= (E_b)_{\theta,\phi}\\ (H_i + H_a)_{\theta,\phi} &= (H_b)_{\theta,\phi}\end{aligned} \tag{18}$$

In the outer space of the particle interface, the electric wave is

$$(E_i + E_{ar})_{\theta,\phi} = M_{o1n}[j_n(k_a r) - \beta_{an}h_n^{(1)}(k_a r)] + N_{e1n}[-i\cdot J_n(k_a r) + i\cdot\alpha_{an}H_n^{(1)}(k_a r)] \tag{19}$$

Where

$$J_n(\rho) = \frac{1}{\rho}\cdot\frac{d}{d\rho}[\rho\cdot j_n(\rho)]$$

$$H_n(\rho) = \frac{1}{\rho}\cdot\frac{d}{d\rho}[\rho\cdot h_n(\rho)] \tag{20}$$

r is the particle's radium. While in the inner space of the particle interface, we have

$$(E_b)_{\theta,\phi} = M_{o1n}[\beta_{bn}j_n(k_b r)] + N_{e1n}[-i\cdot\alpha_{bn}J_n(k_b r)] \tag{21}$$

In terms of (18), we have

$$\begin{aligned}\beta_{an}h_n^{(1)}(k_a r) + \beta_{bn}j_n(k_b r) &= j_n(k_a r)\\ \alpha_{an}H_n^{(1)}(k_a r) + \alpha_{bn}J_n(k_b r) &= J_n(k_a r)\end{aligned} \tag{22}$$

In the outer space of the particle, the magnetic wave is

$$(H_i + H_{ar})_{\theta,\phi} = \frac{k_a}{\omega\mu_a} N_{o1n}[-i \cdot j_n(k_a r) + i \cdot \beta_{an} h_n^{(1)}(k_a r)] + \frac{k_a}{\omega\mu_a} M_{e1n}[-J_n(k_a r) + \alpha_{an} H_n^{(1)}(k_a r)] \quad (23)$$

While in the inner space of the particle interface, we have

$$(H_b)_{\theta,\phi} = -\frac{k_b}{\omega\mu_b} N_{o1n}[i \cdot \beta_{bn} j_n(k_b r)] - \frac{k_b}{\omega\mu_b} M_{e1n}[\alpha_{bn} J_n(k_b r)] \quad (24)$$

In terms of (18), we have

$$\begin{aligned} &\beta_{an} h_n^{(1)}(k_a r) + \beta_{bn} K \cdot j_n(k_b r) = j_n(k_a r) \\ &\alpha_{an} H_n^{(1)}(k_a r) + \alpha_{bn} K \cdot J_n(k_b r) = J_n(k_a r) \\ &K = \frac{k_b}{k_a}\left(\frac{\mu_a}{\mu_b}\right) \end{aligned} \quad (25)$$

With the four equations inserted into the boundary conditions, $r = r_b$, the four constants α_{an}, β_{an}, α_{cn}, β_{cn} are in determinate form,

$$\alpha_{an} = \frac{\begin{bmatrix} \frac{k_a}{\mu} \cdot j_n(k_a r_b) & \frac{k_b}{\mu} \cdot j_n(k_b r_b) \\ (n+1)\frac{j_n(k_a r_b)}{k_a r_b} - j_{n+1}(k_a r_b) & (n+1)\frac{j_n(k_b r_b)}{k_b r_b} - j_{n+1}(k_b r_b) \end{bmatrix}}{\begin{bmatrix} \frac{k_a}{\mu} \cdot h_n(k_a r_b) & \frac{k_b}{\mu} \cdot j_n(k_b r_b) \\ (n+1)\frac{h_n(k_a r_b)}{k_a r_b} - h_{n+1}(k_a r_b) & (n+1)\frac{j_n(k_b r_b)}{k_b r_b} - j_{n+1}(k_b r_b) \end{bmatrix}}$$

$$\beta_{an}=\frac{\begin{bmatrix} j_n(k_a r_b) & j_n(k_b r_b) \\ \frac{k_a}{\mu}[(n+1)\frac{j_n(k_a r_b)}{k_a r_b}-j_{n+1}(k_a r_b)] & \frac{k_b}{\mu}[(n+1)\frac{j_n(k_b r_b)}{k_b r_b}-j_{n+1}(k_b r_b)] \end{bmatrix}}{\begin{bmatrix} h_n(k_a r_b) & j_n(k_b r_b) \\ \frac{k_a}{\mu}\cdot[(n+1)\frac{h_n(k_a r_b)}{k_a r_b}-h_{n+1}(k_a r_b)] & \frac{k_b}{\mu}\cdot[(n+1)\frac{j_n(k_b r_b)}{k_b r_b}-j_{n+1}(k_b r_b)] \end{bmatrix}}$$

$$\beta_{bn}=\frac{\begin{bmatrix} h_n(k_a r_b) & j_n(k_a r_b) \\ \frac{k_a}{\mu}[(n+1)\frac{h_n(k_a r_b)}{k_a r_b}-h_{n+1}(k_a r_b)] & \frac{k_a}{\mu}[(n+1)\frac{j_n(k_a r_b)}{k_a r_b}-j_{n+1}(k_a r_b)] \end{bmatrix}}{\begin{bmatrix} h_n(k_a r_b) & j_n(k_b r_b) \\ \frac{k_a}{\mu}\cdot[(n+1)\frac{h_n(k_a r_b)}{k_a r_b}-h_{n+1}(k_a r_b)] & \frac{k_b}{\mu}\cdot[(n+1)\frac{j_n(k_b r_b)}{k_b r_b}-j_{n+1}(k_b r_b)] \end{bmatrix}}$$

$$\alpha_{bn}=\frac{\begin{bmatrix} \frac{k_a}{\mu}\cdot h_n(k_a r_b) & \frac{k_a}{\mu}\cdot j_n(k_a r_b) \\ (n+1)\frac{h_n(k_a r_b)}{k_a r_b}-j_{n+1}(k_a r_b) & (n+1)\frac{j_n(k_a r_b)}{k_a r_b}-j_{n+1}(k_a r_b) \end{bmatrix}}{\begin{bmatrix} \frac{k_a}{\mu}\cdot h_n(k_a r_b) & \frac{k_b}{\mu}\cdot j_n(k_b r_b) \\ (n+1)\frac{h_n(k_a r_b)}{k_a r_b}-h_{n+1}(k_a r_b) & (n+1)\frac{j_n(k_b r_b)}{k_b r_b}-j_{n+1}(k_b r_b) \end{bmatrix}} \tag{26}$$

Where $\mu_a=1$ for air and we set $\mu_b=\mu$. With α_{an}, β_{an}, α_{cn}, β_{cn} calculated and E_n obtained for the case of the focused beam, all electric and magnetic fields as a function of (r_p,θ_p,ϕ_p) are given.

4.3 Nanoshell Case

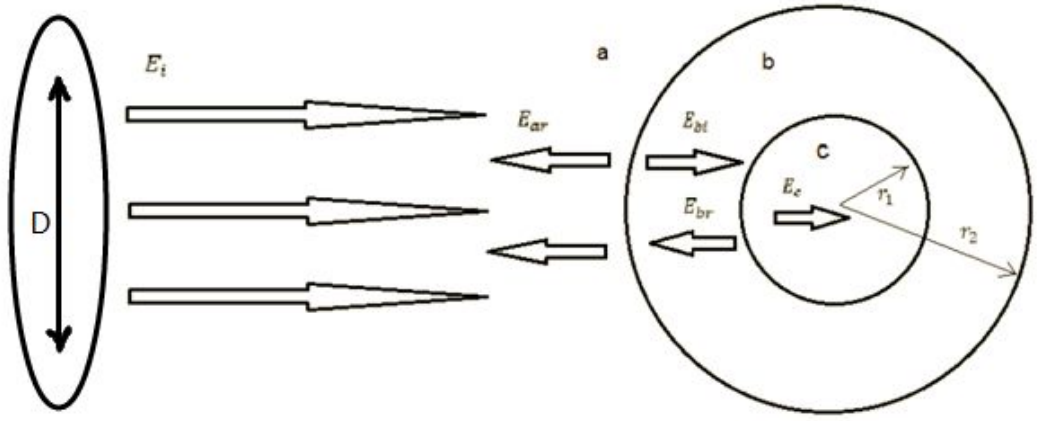

Figure 7. The schematic of beam incident on the nanoshell

For the case of the beam incident on the nanoshell made of a dialectic particle with a radium of r_1 covered with a gold shell with a total radium of r_2. As well, E_i is the incident beam, and we also use the spherical Hankel function of the first kind to describe the scattered field E_{ar} and E_{br} by the a, b interface and b, c interface : $h_n^{(1)}(\rho)$ with $h_n^{(1)}(\rho) \equiv j_n(\rho) + i \cdot y_n(\rho)$. We use the spherical Hankel function of the second kind to describe the incident field E_{bi} into the particle b : $h_n^{(2)}(\rho)$ with $h_n^{(2)}(\rho) \equiv j_n(\rho) - i \cdot y_n(\rho)$. E_c is the transmitted beam into the spherical particle with a radium of r_2 described by the spherical Bessel function $j_n(\rho)$ like E_i since $h_n(\rho)$ diverges at $\rho = 0$. All the radius of the sphere are assumed to increased to infinity, so

that part of it would be reduced to a planar layer problem. We set the right is the positive direction.

Expansion of incident electric field in spherical coordinates is given as below,

$$E_i = \sum_{n=1}^{\infty} E_n (M_{o1n}^{(0)} - i \cdot N_{e1n}^{(0)}) \tag{27}$$

The E_n in the plane wave is given by $E_n = E_0 \cdot i^n \cdot \frac{2n+1}{n(n+1)}$. Since the magnetic wave

$$H_i = \frac{1}{i\omega\mu_a} \nabla \times E_i = \frac{1}{i\omega\mu_a} \sum_{n=1}^{\infty} E_n (\nabla \times M_{o1n}^{(0)} - i \cdot \nabla \times N_{e1n}^{(0)}) \tag{28}$$

We can use

$$\nabla \times N = k \cdot M$$

$$\nabla \times M = k \cdot N$$

$$k^2 = i\omega\mu \cdot (\sigma - i\omega\varepsilon)$$

$$\sigma = 0 \tag{29}$$

We can get

$$H_i = -\frac{k_a}{\omega\mu_a} \sum_{n=1}^{\infty} E_n (M_{e1n}^{(0)} + i \cdot N_{o1n}^{(0)}) \tag{30}$$

Also, the reflected electric and magnetic wave by the particle surface are

$$E_{ar} = \sum_{n=1}^{\infty} E_n (i \cdot \alpha_{an} N_{e1n}^{(1)} - \beta_{an} M_{o1n}^{(1)})$$

$$H_{ar} = \frac{k_a}{\omega\mu_a}\sum_{n=1}^{\infty} E_n(i\cdot\beta_{an}N_{o1n}^{(1)} + \alpha_{an}M_{e1n}^{(1)}) \tag{31}$$

Where (0), (1) means the use of Bessel function and Hankel function. In the metal region, we have

$$E_b = \sum_{n=1}^{\infty} E_n(\beta_{bn}^{(1)}M_{o1n}^{(1)} + \beta_{bn}^{(2)}M_{o1n}^{(2)} - i\cdot\alpha_{bn}^{(1)}M_{o1n}^{(1)} - i\cdot\alpha_{bn}^{(2)}M_{o1n}^{(2)})$$

$$H_b = \frac{k_b}{\omega\mu_b}\sum_{n=1}^{\infty} E_n(i\cdot\beta_{bn}^{(1)}N_{o1n}^{(1)} + i\cdot\beta_{bn}^{(2)}N_{o1n}^{(2)} + \alpha_{bn}^{(1)}M_{e1n}^{(1)} + \alpha_{bn}^{(2)}M_{e1n}^{(2)}) \tag{32}$$

Which consist of the incident and the scattered field in the b region with $k_b^2 = i\omega\mu_b\cdot(\sigma_b - i\omega\varepsilon_b)$. In the core region, we only have Bessel beam because the Hankel beam diverges at $\rho = 0$:

$$E_c = \sum_{n=1}^{\infty} E_n(\beta_{cn}M_{o1n}^{(0)} - i\cdot\alpha_{cn}N_{e1n}^{(0)})$$

$$H_c = -\frac{k_c}{\omega\mu_c}\sum_{n=1}^{\infty} E_n(i\cdot\beta_{cn}N_{o1n}^{(0)} + \alpha_{cn}M_{e1n}^{(0)}) \tag{33}$$

Thus we have eight constants to be determined: α_{an}, β_{an}, $\alpha_{bn}^{(1)}$, $\beta_{bn}^{(1)}$, $\alpha_{bn}^{(2)}$, $\beta_{bn}^{(2)}$, α_{cn}, β_{cn}. According to formula (5), if the manuscript is (0), replace $z_n(\rho)$ into $j_n(\rho)$; if the manuscript is (1), replace $z_n(\rho)$ into $h_n^{(1)}(\rho)$; if the manuscript is (2), replace $z_n(\rho)$ into $h_n^{(2)}(\rho)$. For the interface of a, b, the tangential components of the electric and magnetic fields in the e_θ and e_ϕ direction must be equal at the particle-medium interface. This equality condition on E and H are expressed as:

$$(E_i + E_a)_{\theta,\phi} = (E_b)_{\theta,\phi}$$

$$(H_i + H_a)_{\theta,\phi} = (H_b)_{\theta,\phi} \tag{34}$$

In the outer space of the nanoshell interface, the electric wave is

$$(E_i + E_{ar})_{\theta,\phi} = M_{o1n}[j_n(k_a r_2) - \beta_{an} h_n^{(1)}(k_a r_2)] + N_{e1n}[-i \cdot J_n(k_a r_2) + i \cdot \alpha_{an} H_n^{(1)}(k_a r_2)] \tag{35}$$

Combines with formula (20) and r_2 is the shell's radium.

In the middle of metal shell space, the electric wave is

$$(E_b)_{\theta,\phi} = M_{o1n}[\beta_{bn}^{(1)} h_n^{(1)}(k_b r_2) + \beta_{bn}^{(2)} h_n^{(2)}(k_b r_2)] + N_{e1n}[-i \cdot \alpha_{bn}^{(1)} H_n^{(1)}(k_b r_2) - i \cdot \alpha_{bn}^{(2)} H_n^{(2)}(k_b r_2)] \tag{36}$$

In terms of (34), we have

$$\begin{aligned} \beta_{an} h_n^{(1)}(k_a r_2) + \beta_{bn}^{(2)} h_n^{(2)}(k_b r_2) &= j_n(k_a r_2) + \beta_{bn}^{(1)} h_n^{(1)}(k_b r_2) \\ \alpha_{an} H_n^{(1)}(k_a r_2) + \alpha_{bn}^{(2)} H_n(k_b r_2) &= J_n(k_a r_2) + \alpha_{bn}^{(1)} H_n(k_b r_2) \end{aligned} \tag{37}$$

In the outer space of the nanoshell, the magnetic wave is

$$(H_i + H_{ar})_{\theta,\phi} = \frac{k_a}{\omega \mu_a} M_{e1n}[-j_n(k_a r_2) + \alpha_{an} h_n^{(1)}(k_a r_2)] + \frac{k_a}{\omega \mu_a} N_{o1n}[-J_n(k_a r_2) + \beta_{an} H_n(k_a r_2)] \tag{38}$$

While in the inner space of the nanoshell interface, we have

$$(H_b)_{\theta,\phi} = -\frac{k_b}{\omega \mu_b} M_{e1n}[-\alpha_{bn}^{(1)} h_n^{(1)}(k_b r_2) + \alpha_{bn}^{(2)} h_n^{(2)}(k_b r_2)] - \frac{k_b}{\omega \mu_b} N_{o1n}[-i \cdot \beta_{bn}^{(1)} H_n^{(1)}(k_b r_2) + i \cdot \beta_{bn}^{(2)} H_n^{(2)}(k_b r_2)] \tag{39}$$

In terms of (34), we have

$$\begin{aligned} \alpha_{an} h_n^{(1)}(k_a r_2) - \alpha_{bn}^{(1)} K_1 \cdot h_n^{(1)}(k_b r_2) + \alpha_{bn}^{(2)} K_1 \cdot h_n^{(2)}(k_b r_2) &= j_n(k_a r_2) \\ \beta_{an} H_n^{(1)}(k_a r_2) - \beta_{bn}^{(1)} K_1 \cdot H_n^{(1)}(k_b r_2) + \beta_{bn}^{(2)} K_1 \cdot H_n^{(2)}(k_b r_2) &= J_n(k_a r_2) \end{aligned}$$

$$K_1 = \frac{k_b}{k_a}\left(\frac{\mu_a}{\mu_b}\right) \tag{40}$$

For the interface of b, c, the tangential components of the electric and magnetic fields in the e_θ and e_ϕ direction must be equal at the particle-medium interface. This equality condition on E and H are expressed as:

$$\begin{aligned}(E_b)_{\theta,\phi} &= (E_c)_{\theta,\phi} \\ (H_b)_{\theta,\phi} &= (H_c)_{\theta,\phi}\end{aligned} \tag{41}$$

In the metal space of the nanoshell interface, the electric wave is

$$(E_b)_{\theta,\phi} = M_{o1n}[\beta_{bn}^{(1)} h_n^{(1)}(k_b r_1) - \beta_{bn}^{(2)} h_n^{(2)}(k_b r_1)] + N_{e1n}[-i \cdot \alpha_{bn}^{(1)} H_n^{(1)}(k_b r_1) + i \cdot \alpha_{bn}^{(2)} H_n^{(2)}(k_b r_1)] \tag{42}$$

In the core space of the nanoshell, the electric wave is

$$(E_c)_{\theta,\phi} = M_{o1n}[\beta_{cn} j_n(k_c r_1)] + N_{e1n}[-i \cdot \alpha_{cn} J_n(k_c r_1)] \tag{43}$$

In terms of (41), we have

$$\begin{aligned}\beta_{cn} j_n(k_c r_1) + \beta_{bn}^{(1)} h_n^{(1)}(k_b r_1) &= \beta_{bn}^{(2)} h_n^{(2)}(k_b r_1) \\ \alpha_{cn} J_n(k_c r_1) + \alpha_{bn}^{(1)} H_n^{(1)}(k_b r_1) &= \alpha_{bn}^{(2)} H_n^{(2)}(k_b r_1)\end{aligned} \tag{44}$$

In the metal space of the nanoshell interface, the magnetic wave is

$$(H_b)_{\theta,\phi} = -\frac{k_b}{\omega \mu_b} M_{e1n}[\alpha_{bn}^{(1)} h_n^{(1)}(k_b r_1) + i \cdot \alpha_{bn}^{(2)} h_n^{(2)}(k_b r_1)] - \frac{k_b}{\omega \mu_b} N_{o1n}[-i \cdot \beta_{bn}^{(1)} H_n^{(1)}(k_b r_1) + i \cdot \beta_{bn}^{(2)} H_n^{(2)}(k_b r_1)] \tag{45}$$

In the core space of the nanoshell, the magnetic wave is

$$(H_c)_{\theta,\phi} = -\frac{k_c}{\omega \mu_c} M_{e1n}[\alpha_{cn} j_n(k_c r_1)] - \frac{k_c}{\omega \mu_c} N_{o1n}[i \cdot \beta_{cn} J_n(k_c r_1)] \tag{46}$$

In terms of (41), we have

$$K_2\alpha_{cn}j_n(k_cr_1)+\alpha_{bn}^{(1)}h_n^{(1)}(k_br_1)=\alpha_{bn}^{(2)}h_n^{(2)}(k_br_1)$$

$$K_2\beta_{cn}J_n(k_cr_1)+\beta_{bn}^{(1)}H_n^{(1)}(k_br_1)=\beta_{bn}^{(2)}H_n^{(2)}(k_br_1)$$

$$K_2=\frac{k_c}{k_b}\left(\frac{\mu_b}{\mu_c}\right) \tag{47}$$

With the eight boundary equations, the eight constants α_{an}, β_{an}, $\alpha_{bn}^{(1)}$, $\beta_{bn}^{(1)}$, $\alpha_{bn}^{(2)}$, $\beta_{bn}^{(2)}$, α_{cn}, β_{cn} are in determinate form,

$$\alpha_{an}=\frac{\begin{bmatrix} \frac{k_a}{\mu_a}\cdot j_n(k_ar_2) & \frac{k_b}{\mu_b}\cdot h_n^{(1)}(k_br_2) & \frac{k_b}{\mu_b}\cdot h_n^{(2)}(k_br_2) & 0 \\ J_n(k_ar_2) & H_n^{(1)}(k_br_2) & H_n^{(2)}(k_br_2) & 0 \\ 0 & \frac{k_b}{\mu_b}\cdot h_n^{(1)}(k_br_1) & \frac{k_b}{\mu_b}\cdot h_n^{(2)}(k_br_1) & -\frac{k_c}{\mu_c}\cdot j_n(k_cr_1) \\ 0 & H_n^{(1)}(k_br_1) & H_n^{(2)}(k_br_1) & -J_n(k_cr_1) \end{bmatrix}}{\begin{bmatrix} \frac{k_a}{\mu_a}\cdot h_n^{(1)}(k_ar_2) & \frac{k_b}{\mu_b}\cdot h_n^{(1)}(k_br_2) & \frac{k_b}{\mu_b}\cdot h_n^{(2)}(k_br_2) & 0 \\ H_n^{(1)}(k_ar_2) & H_n^{(1)}(k_br_2) & H_n^{(2)}(k_br_2) & 0 \\ 0 & \frac{k_b}{\mu_b}\cdot h_n^{(1)}(k_br_1) & \frac{k_b}{\mu_b}\cdot h_n^{(2)}(k_br_1) & -\frac{k_c}{\mu_c}\cdot j_n(k_cr_1) \\ 0 & H_n^{(1)}(k_br_1) & H_n^{(2)}(k_br_1) & -J_n(k_cr_1) \end{bmatrix}}$$

$$\beta_{an}=\frac{\begin{bmatrix} j_n(k_a r_2) & -h_n^{(1)}(k_b r_2) & h_n^{(2)}(k_b r_2) & 0 \\ \frac{k_a}{\mu_a}\cdot H_n^{(1)}(k_a r_2) & -\frac{k_b}{\mu_b}\cdot H_n^{(1)}(k_b r_2) & \frac{k_b}{\mu_b}\cdot H_n^{(2)}(k_b r_2) & 0 \\ 0 & -h_n^{(1)}(k_b r_1) & h_n^{(2)}(k_b r_1) & -j_n(k_c r_1) \\ 0 & -\frac{k_b}{\mu_b}\cdot H_n^{(1)}(k_b r_1) & \frac{k_b}{\mu_b}\cdot H_n^{(2)}(k_b r_1) & -\frac{k_c}{\mu_c}\cdot J_n(k_c r_1) \end{bmatrix}}{\begin{bmatrix} h_n^{(1)}(k_a r_2) & -h_n^{(1)}(k_b r_2) & h_n^{(2)}(k_b r_2) & 0 \\ \frac{k_a}{\mu_a}\cdot H_n^{(1)}(k_a r_2) & -\frac{k_b}{\mu_b}\cdot H_n^{(1)}(k_b r_2) & \frac{k_b}{\mu_b}\cdot H_n^{(2)}(k_b r_2) & 0 \\ 0 & -h_n^{(1)}(k_b r_1) & h_n^{(2)}(k_b r_1) & -j_n(k_c r_1) \\ 0 & -\frac{k_b}{\mu_b}\cdot H_n^{(1)}(k_b r_1) & \frac{k_b}{\mu_b}\cdot H_n^{(2)}(k_b r_1) & -\frac{k_c}{\mu_c}\cdot J_n(k_c r_1) \end{bmatrix}}$$

$$\alpha_{bn}^{(1)}=\frac{\begin{bmatrix} \frac{k_a}{\mu_a}\cdot h_n^{(1)}(k_a r_2) & \frac{k_b}{\mu_b}\cdot j_n(k_b r_2) & \frac{k_b}{\mu_b}\cdot h_n^{(2)}(k_b r_2) & 0 \\ H_n^{(1)}(k_a r_2) & J_n(k_b r_2) & H_n^{(2)}(k_b r_2) & 0 \\ 0 & 0 & \frac{k_b}{\mu_b}\cdot h_n^{(2)}(k_b r_1) & -\frac{k_c}{\mu_c}\cdot j_n(k_c r_1) \\ 0 & 0 & H_n^{(2)}(k_b r_1) & -J_n(k_c r_1) \end{bmatrix}}{\begin{bmatrix} \frac{k_a}{\mu_a}\cdot h_n^{(1)}(k_a r_2) & -\frac{k_b}{\mu_b}\cdot h_n^{(1)}(k_b r_2) & \frac{k_b}{\mu_b}\cdot h_n^{(2)}(k_b r_2) & 0 \\ H_n^{(1)}(k_a r_2) & -H_n^{(1)}(k_b r_2) & H_n^{(2)}(k_b r_2) & 0 \\ 0 & -\frac{k_b}{\mu_b}\cdot h_n^{(1)}(k_b r_1) & \frac{k_b}{\mu_b}\cdot h_n^{(2)}(k_b r_1) & -\frac{k_c}{\mu_c}\cdot j_n(k_c r_1) \\ 0 & -H_n^{(1)}(k_b r_1) & H_n^{(2)}(k_b r_1) & -J_n(k_c r_1) \end{bmatrix}}$$

$$\beta_{bn}^{(1)}=\frac{\begin{bmatrix} h_n^{(1)}(k_a r_2) & j_n(k_a r_2) & h_n^{(2)}(k_b r_2) & 0 \\ \frac{k_a}{\mu_a}\cdot H_n^{(1)}(k_a r_2) & \frac{k_a}{\mu_a}\cdot J_n(k_a r_2) & \frac{k_b}{\mu_b}\cdot H_n^{(2)}(k_b r_2) & 0 \\ 0 & 0 & h_n^{(2)}(k_b r_1) & -j_n(k_c r_1) \\ 0 & 0 & \frac{k_b}{\mu_b}\cdot H_n^{(2)}(k_b r_1) & -\frac{k_c}{\mu_c}\cdot J_n(k_c r_1) \end{bmatrix}}{\begin{bmatrix} h_n^{(1)}(k_a r_2) & -h_n^{(1)}(k_b r_2) & h_n^{(2)}(k_b r_2) & 0 \\ \frac{k_a}{\mu_a}\cdot H_n^{(1)}(k_a r_2) & -\frac{k_b}{\mu_b}\cdot H_n^{(1)}(k_b r_2) & \frac{k_b}{\mu_b}\cdot H_n^{(2)}(k_b r_2) & 0 \\ 0 & -h_n^{(1)}(k_b r_1) & h_n^{(2)}(k_b r_1) & -j_n(k_c r_1) \\ 0 & -\frac{k_b}{\mu_b}\cdot H_n^{(1)}(k_b r_1) & \frac{k_b}{\mu_b}\cdot H_n^{(2)}(k_b r_1) & -\frac{k_c}{\mu_c}\cdot J_n(k_c r_1) \end{bmatrix}}$$

$$\alpha_{bn}^{(2)} = \frac{\begin{bmatrix} \frac{k_a}{\mu_a}\cdot h_n^{(1)}(k_a r_2) & -\frac{k_b}{\mu_b}\cdot h_n^{(1)}(k_b r_2) & \frac{k_b}{\mu_b}\cdot j_n(k_a r_2) & 0 \\ H_n^{(1)}(k_a r_2) & -H_n^{(1)}(k_b r_2) & J_n(k_a r_2) & 0 \\ 0 & -\frac{k_b}{\mu_b}\cdot h_n^{(1)}(k_b r_1) & 0 & -\frac{k_c}{\mu_c}\cdot j_n(k_c r_1) \\ 0 & -H_n^{(1)}(k_b r_1) & 0 & -J_n(k_c r_1) \end{bmatrix}}{\begin{bmatrix} \frac{k_a}{\mu_a}\cdot h_n^{(1)}(k_a r_2) & -\frac{k_b}{\mu_b}\cdot h_n^{(1)}(k_b r_2) & \frac{k_b}{\mu_b}\cdot h_n^{(2)}(k_b r_2) & 0 \\ H_n^{(1)}(k_a r_2) & -H_n^{(1)}(k_b r_2) & H_n^{(2)}(k_b r_2) & 0 \\ 0 & -\frac{k_b}{\mu_b}\cdot h_n^{(1)}(k_b r_1) & \frac{k_b}{\mu_b}\cdot h_n^{(2)}(k_b r_1) & -\frac{k_c}{\mu_c}\cdot j_n(k_c r_1) \\ 0 & -H_n^{(1)}(k_b r_1) & H_n^{(2)}(k_b r_1) & -J_n(k_c r_1) \end{bmatrix}}$$

$$\beta_{bn}^{(2)} = \frac{\begin{bmatrix} h_n^{(1)}(k_a r_2) & -h_n^{(1)}(k_b r_2) & j_n(k_a r_2) & 0 \\ \frac{k_a}{\mu_a}\cdot H_n^{(1)}(k_a r_2) & -\frac{k_b}{\mu_b}\cdot H_n^{(1)}(k_b r_2) & \frac{k_a}{\mu_a}\cdot J_n(k_a r_2) & 0 \\ 0 & -h_n^{(1)}(k_b r_1) & 0 & -j_n(k_c r_1) \\ 0 & -\frac{k_b}{\mu_b}\cdot H_n^{(1)}(k_b r_1) & 0 & -\frac{k_c}{\mu_c}\cdot J_n(k_c r_1) \end{bmatrix}}{\begin{bmatrix} h_n^{(1)}(k_a r_2) & -h_n^{(1)}(k_b r_2) & h_n^{(2)}(k_b r_2) & 0 \\ \frac{k_a}{\mu_a}\cdot H_n^{(1)}(k_a r_2) & -\frac{k_b}{\mu_b}\cdot H_n^{(1)}(k_b r_2) & \frac{k_b}{\mu_b}\cdot H_n^{(2)}(k_b r_2) & 0 \\ 0 & -h_n^{(1)}(k_b r_1) & h_n^{(2)}(k_b r_1) & -j_n(k_c r_1) \\ 0 & -\frac{k_b}{\mu_b}\cdot H_n^{(1)}(k_b r_1) & \frac{k_b}{\mu_b}\cdot H_n^{(2)}(k_b r_1) & -\frac{k_c}{\mu_c}\cdot J_n(k_c r_1) \end{bmatrix}}$$

$$\alpha_{cn}=\frac{\begin{bmatrix} \frac{k_a}{\mu_a}\cdot h_n^{(1)}(k_a r_2) & -\frac{k_b}{\mu_b}\cdot h_n^{(1)}(k_b r_2) & \frac{k_b}{\mu_b}\cdot h_n^{(2)}(k_b r_2) & \frac{k_b}{\mu_b}\cdot j_n(k_a r_2) \\ H_n^{(1)}(k_a r_2) & -H_n^{(1)}(k_b r_2) & H_n^{(2)}(k_b r_2) & J_n(k_a r_2) \\ 0 & -\frac{k_b}{\mu_b}\cdot h_n^{(1)}(k_b r_1) & \frac{k_b}{\mu_b}\cdot h_n^{(2)}(k_b r_1) & 0 \\ 0 & -H_n^{(1)}(k_b r_1) & H_n^{(2)}(k_b r_1) & 0 \end{bmatrix}}{\begin{bmatrix} \frac{k_a}{\mu_a}\cdot h_n^{(1)}(k_a r_2) & -\frac{k_b}{\mu_b}\cdot h_n^{(1)}(k_b r_2) & \frac{k_b}{\mu_b}\cdot h_n^{(2)}(k_b r_2) & 0 \\ H_n^{(1)}(k_a r_2) & -H_n^{(1)}(k_b r_2) & H_n^{(2)}(k_b r_2) & 0 \\ 0 & -\frac{k_b}{\mu_b}\cdot h_n^{(1)}(k_b r_1) & \frac{k_b}{\mu_b}\cdot h_n^{(2)}(k_b r_1) & -\frac{k_c}{\mu_c}\cdot j_n(k_c r_1) \\ 0 & -H_n^{(1)}(k_b r_1) & H_n^{(2)}(k_b r_1) & -J_n(k_c r_1) \end{bmatrix}}$$

$$\beta_{cn}=\frac{\begin{bmatrix} h_n^{(1)}(k_a r_2) & -h_n^{(1)}(k_b r_2) & h_n^{(2)}(k_b r_2) & j_n(k_a r_2) \\ \frac{k_a}{\mu_a}\cdot H_n^{(1)}(k_a r_2) & -\frac{k_b}{\mu_b}\cdot H_n^{(1)}(k_b r_2) & \frac{k_b}{\mu_b}\cdot H_n^{(2)}(k_b r_2) & \frac{k_a}{\mu_a}\cdot J_n(k_a r_2) \\ 0 & -h_n^{(1)}(k_b r_1) & h_n^{(2)}(k_b r_1) & 0 \\ 0 & -\frac{k_b}{\mu_b}\cdot H_n^{(1)}(k_b r_1) & \frac{k_b}{\mu_b}\cdot H_n^{(2)}(k_b r_1) & 0 \end{bmatrix}}{\begin{bmatrix} h_n^{(1)}(k_a r_2) & -h_n^{(1)}(k_b r_2) & h_n^{(2)}(k_b r_2) & 0 \\ \frac{k_a}{\mu_a}\cdot H_n^{(1)}(k_a r_2) & -\frac{k_b}{\mu_b}\cdot H_n^{(1)}(k_b r_2) & \frac{k_b}{\mu_b}\cdot H_n^{(2)}(k_b r_2) & 0 \\ 0 & -h_n^{(1)}(k_b r_1) & h_n^{(2)}(k_b r_1) & -j_n(k_c r_1) \\ 0 & -\frac{k_b}{\mu_b}\cdot H_n^{(1)}(k_b r_1) & \frac{k_b}{\mu_b}\cdot H_n^{(2)}(k_b r_1) & -\frac{k_c}{\mu_c}\cdot J_n(k_c r_1) \end{bmatrix}} \quad (48)$$

5. NANOJET CALCULATIONS

5.1 Case One

We present calculations of nanojets at a wavelength of 400 nm. The particle is assumed to be a fused silica particle with a diameter of 2 um and a refractive index of 1.47 at 400 nm wavelength. Figure 4a and 4a' show the nanojet formed when the focal point and the center of the particle are at the same point for the case corresponding to NA=0.4. The width of the nanojet waist is a function of the azimuthal angle ϕ. Figure 4a is for the case $\phi = \pi/2$, which corresponds to the plane perpendicular to the plane formed by the incident electric field polarization and its propagation direction. The electric field intensity normalized to the focal intensity versus r_p is shown below for θ_p =0 and for θ_p =0.115 when the intensity drops by one-half at the nanojet waist. From θ_p =0.115, the calculated FWHM of the waist is about 253 nm. Figure 4a' is for the case ϕ = 0, which correspond to the plane formed by the incident field polarization and its propagation direction. The half intensity occurs at θ_p=0.145 as shown, which indicates that the FWHM of the waist is 319 nm. Figure 4b and 4b' show the nanojet formed when the center of the particle is 3.9 um away from the focal point. Compared with figure 4a and a', it is observed that the nanojet moved away from the surface of the particle by 215 nm. For $\phi = \pi/2$, the half intensity occurs at θ_p = 0.102 which indicates that the FWHM of the waist is about 245 nm. For ϕ= 0, the FWHM is 316 nm. Thus the width of the waist remains about the same for the same ϕ but the position of the waist is moved farther outside the particle. Note that the nanojet field intensity is slightly smaller for figure 4b and b' than for figure 4a and a' because when the particle is displaced from the focal

point, the FWHM of the incident beam at the particle is 1.2 um rather than 0.84 um; ie the particle collects less light. The asymmetry of the nanojet waist with respect to ϕ should be alleviated for circular polarization because the x or the y incident field polarization component is largely maintained during propagation.

Figure (c), (c'), (d), and (d') are cases when the NA =0.8. For (c) and (c'), the particle is at the focal point. The nanojet waist is inside the particle. For (d) and (d'), the particle is 3.9 um away from the focal point. The nanojet waist is now 335 nm outside the particle. For $\phi = \frac{\pi}{2}$, the FWHM of the waist is 256 nm, and for $\phi = 0$, it is 315 nm. Thus, the FWHM of the waist are roughly the same for NA=0.4 and NA=0.8,

In figure 4e and 4e', the result for the case of a plane wave incident field, as generally assumed, is also calculated and compared with the focused beam case. It is noted that for $\phi = \frac{\pi}{2}$, the FWHM of the beam waist is as narrow as 150 nm and occurs at the surface of the particle. However, for $\phi = 0$, the FWHM is 340 nm. Thus, the focused beam analysis produce a less asymmetric results compared with the plane wave analysis.

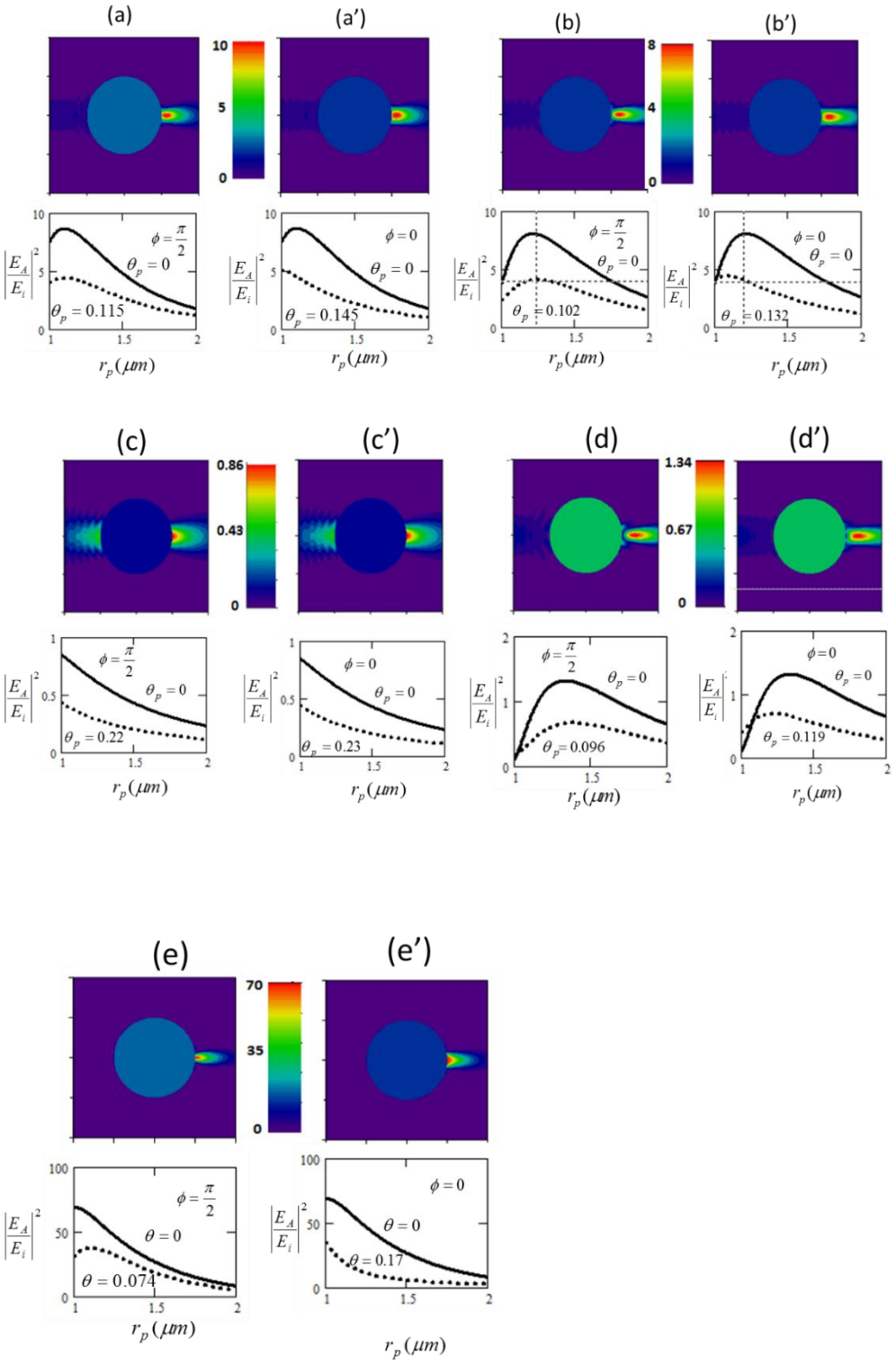

Figure 8. The nanojet pictures and plots for different situations.

It is noted that nanojets intensity enhancement for focused beam shown in Figure 8(a) to Figure 8(d) are substantially smaller than for a plane wave beam shown in Figure 8(e). This is reasonable because a nanoparticle collects much more photon for an incident focused beam than a plane wave, which theoretically is of infinite spatial extent. For instance, the intensity enhancement in Figure 8(c) is only about one. If the enhancement were 100, the nanojet beam size would have to shrink to about 25 nm (factor of 10) since the definition of intensity is power/area.

5.2 Case Two

For the case of very small particle size, based on the wavelength of 400 nm and NA of 0.9 for the nanojet calculation, the particle is assumed to be a fused silica particle with a diameter of 50 nm, 100 nm and 200 nm respectively shown in Figure (9). And the particle with different sizes is placed at a distance of 0 nm, 191 nm and 318 nm for both behind and in front of the focal point which gives us five different positions. When the particle with a diameter of 50 nm is placed 191 nm on the right side away from the focal point, the nanojet is not obvious. Using the same method presented in ref[26]. When the particle increases to 100 nm and 200 nm of the diameter, the corresponding FWHM will increase to 123 nm and 159 nm respectively which are all quite beyond the diffraction limit of 222 nm for this

case obviously. The symmetric position of the particle about the focal point which means on the right side 191 nm away from the focal point, the FWHM number will decrease as 218 nm, 208 nm and 168 nm when the particle diameter increases as 50 nm, 100 nm, 200 nm. As the beam waists are both 114 nm at those symmetric positions about the focal point, interestingly, when the particles are chosen to be the same size as the beam waists, the FWHM numbers of them happen to achieve a smallest difference of 12 nm only. The same phenomenon happens when the two positions are 318 nm away from the focal point symmetrically. The shape of nanojets from the particle on the left side of the focal point has a longer shape than the right ones and most of the nanojets are positioned outside the particle which is practical for industry usage.

R=0 (particle at focal point)

(a1) (a2) (a3)

D=50 nm D=100 nm D=200 nm

(FWHM=152 nm) (FWHM=163 nm)

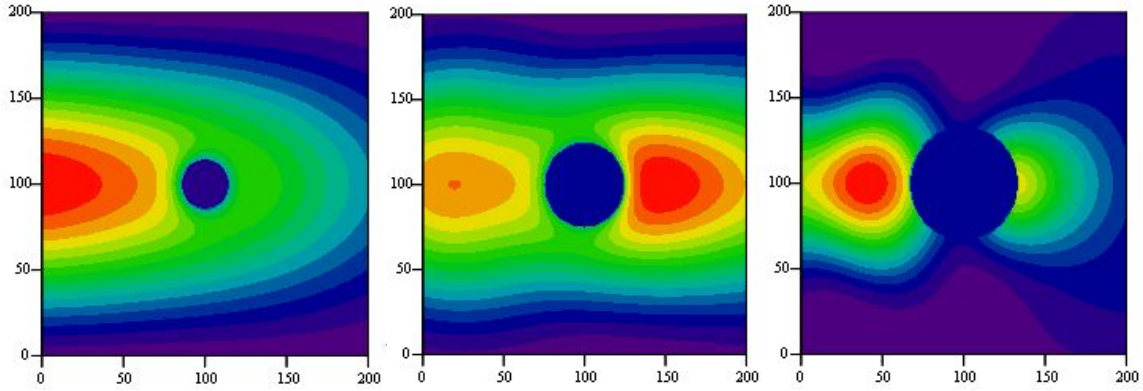

R= 191 nm (particle behind focal point)

(b1) (b2) (b3)

D= 50 nm D= 100nm D=200 nm

(FWHM=159 nm)

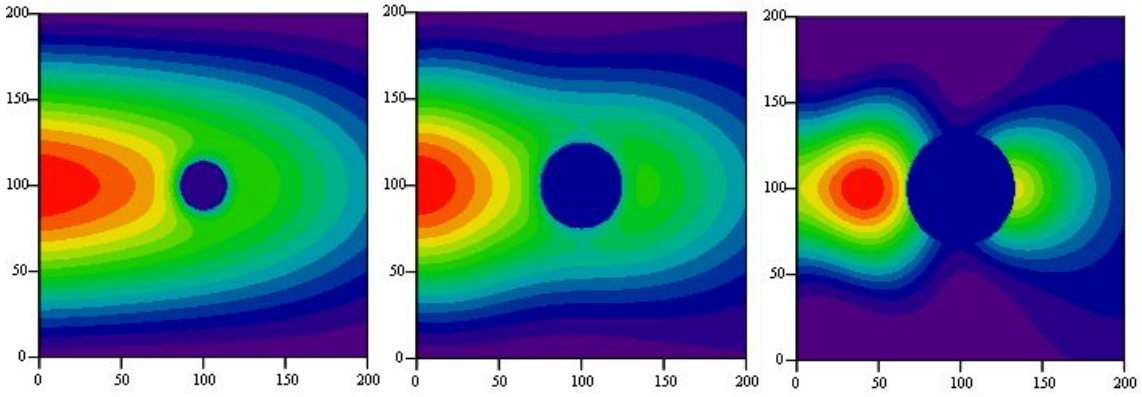

Figure 9: The nanojet pictures and plots for different situations

R= -191 nm (particle in front of focal point)

(c1) (c2) (c3)

D= 50 nm D=100 nm D=200nm

(FWHM=218 nm) (FWHM=208 nm) (FWHM=168 nm)

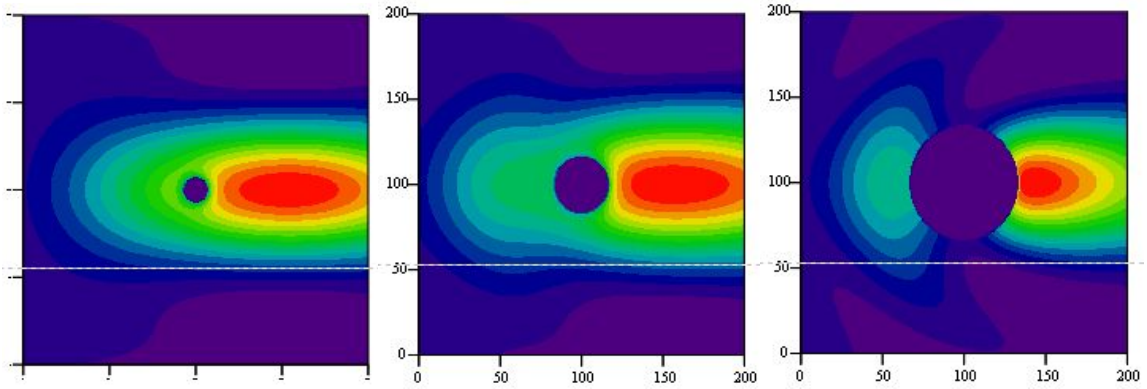

R=318 nm (particle behind focal point)

(d1) (d2) (d3)

D=50 nm D= 100 nm D=200 nm

(FWHM=158 nm) (FWHM=169 nm)

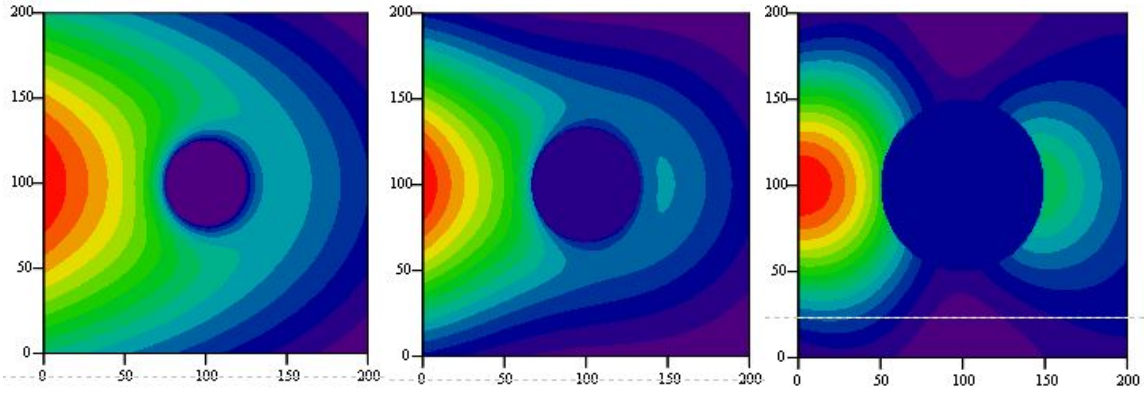

(Figure 9 continued)

R= -318 nm (particle in front of focal point)

(e1) (e2) (e3)

D= 50 nm D= 100 nm D=200 nm

(FWHM=224 nm) (FWHM=222 nm) (FWHM=182 nm)

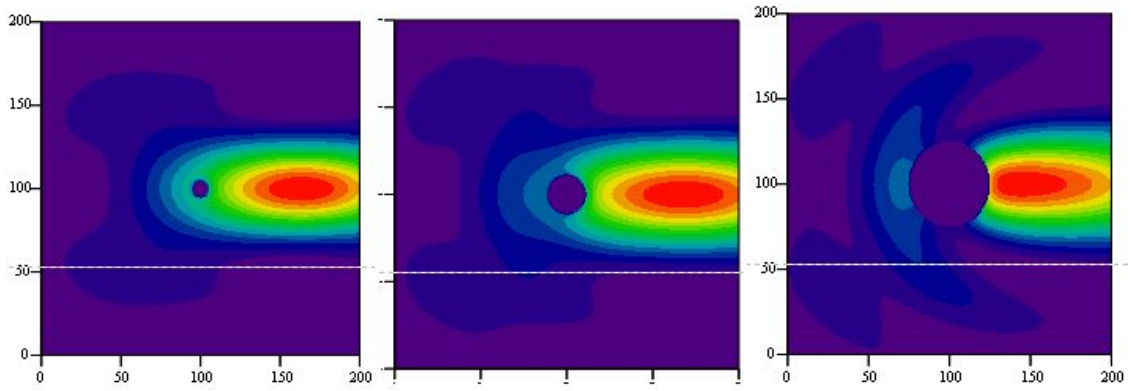

Plane wave case

(f1) (f2)

D=100 nm D=200 nm

(FWHM=215 nm) (FWHM=200 nm)

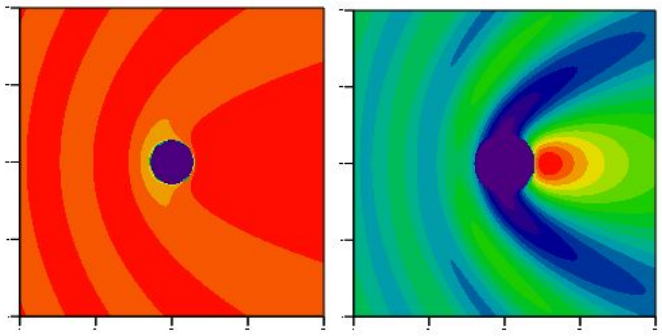

(Figure 9 continued)

Considering the particle exactly on the focal point, it can be compared with the situation of plane-wave incidence. Since the field can be regarded as parallel propagation to the axis near the focal point, the particle can be regarded as being placed in a plane wave environment especially when the particle is small enough. The FWHM of the nanojet waist decreases from 215 nm to 154 nm then increase to 200 nm when the particle diameter increases from 50 nm to 222 nm to 400 nm. Among them, the 222-nm-diameter gives the smallest result which exactly occupies the beam waist of the focal point. Plus, this special size manifests the property of Gaussian beam to the greatest extent. Due to the homogeneity of the plane wave, the FWHM of the nanojet waist changes when the particle size changes in a broader range. As well, the waist achieve the minimum of 130 nm when the diameter of the particle becomes 2 um.

5.3 Case Three

For the case of nanoshells, the dielectic particle is covered with a gold layer 10 nm in thickness. The incident light is a focused beam which is the same as in case two. The positions of the particle are are 318 nm and 636 nm away from the focal point in the direction towards the lens as shown in Figure (10). Specifically, when the nanoshell with a diameter of 220 nm is shifted 318 nm closer to the lens the shape of the nanojet is longer and 330 nm away from the nanoshell center with a FWHM of 225 nm. When the diameter of the nanoshell is 420 nm, the FWHM of the nanojet has a FWHM of 131 nm. And when the diameter of the shell is increased to 620 nm, the nanojet is 896 nm away from the nanoshell center with a FWHM of 201 nm. When the nanoshell is shifted 636

nm away from the focal point (twice the distance as the former case), the nanojets are separated even more away from the nanoshell than the previous ones. Their FWHM are 206.82 nm, 209.04 nm and 211.86 nm corresponding to the nanoshell diameter of 220 nm, 420 nm and 620 nm respectively. And the distance are 642 nm, 671 nm and 764 nm away from the nanoshell centers respectively. If the incident beam is a plane wave and when the diameter of the nanoshell are 1020 nm and 2020 nm, the FWHM of the nanojets are 150 nm and 161 nm respectively, similar to case 2.

R=-318 nm (particle in front of focal point)

(a1) (a2) (a3)

D= 220 nm D=420 nm D= 620 nm

(FWHM=220 nm) (FWHM=131 nm) (FWHM=201 nm)

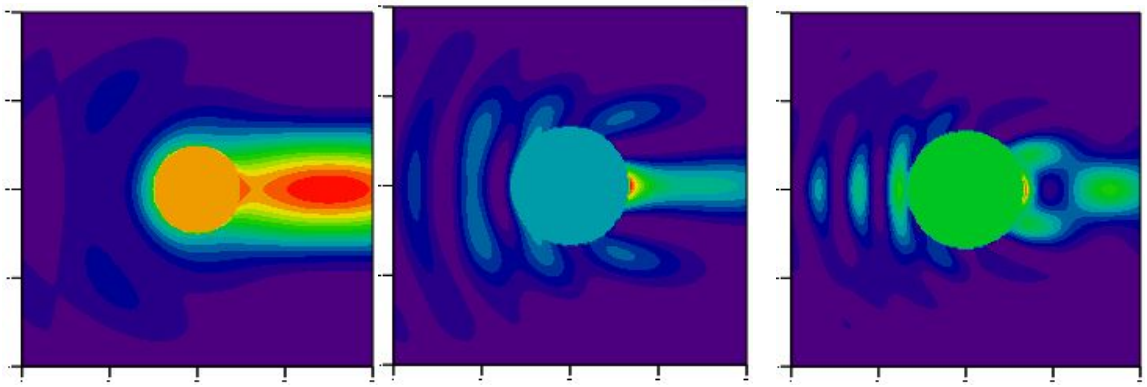

R= -636 (particle in front of focal point)

(b1) (b2) (b3)

D= 220 nm D=420 nm D=620 nm

(FWHM=207 nm) (FWHM=209 nm) (FWHM=212 nm)

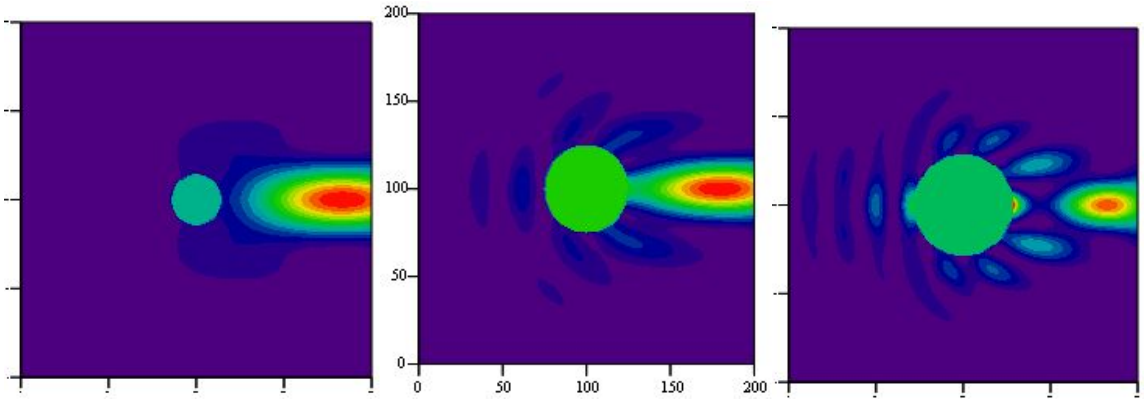

Figure 10: The nanojet pictures and plots for different situations.

Plane wave case

(c1) (c2)

D= 1020 nm D= 2020 nm

(FWHM=150 nm) (FWHM=161 nm)

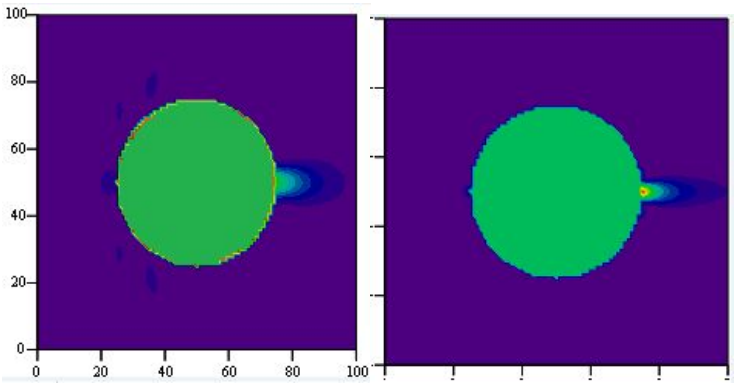

(Figure 10 continued)

6. CONCLUSIONS

The nanojet formed by a focused incident beam with a spot size smaller or comparable to the particle size is studied in the research. We used the vector spherical harmonics expansion of the focused beam to make a rigorous calculation of the 3-D nanojets for the case when the particle center is at or away from the focal point. It is also found that the nanojet spot size is more symmetric with respect to the azimuthal angle than the case if the incident field is a plane wave.

With all the coefficients calculated by the program, the property of the nanojets are manifested naturally. The nanojets can be shifted away from the particle by changing the shape of the focused beam, and the FWHM and length of the nanojets can also be changed by changing the focused beam. The results generated by the focused beam are compared to the plane wave cases.

REFERENCES

[1] Zhigang Chen, Allen Taflove and Vadim Backman 2004 Photonic nanojet enhancement of backscattering of light by nanoparticles : a potential novel visible light ultramicroscopy technique Opt. Express 12, 1214-1220

[2] Xu Li, Zhigang Chen, Allen Taflove, and Vadim Backman 2005 Optical analysis of nanoparticles via enhanced backscattering facilitated 3-D photonic nanojets Opt. Express 13, 526-533

[3] Luk'Yanchuk B. S, Wang Z. B, Song W. D. Hong 2004 Particle on surface: 3D-effects in dry laser cleaning. Applied Physics A, 79, 747-751.

[4] Alexander Heifetz, Soon-Cheik Kong, Alan V. Sahakian, Allen Taflove, and Vadim Backman 2009 Photonic Nanojets J. Comput. Theo. Nanosci. 6, 1979-1991

[5] Kallepalli, L.N.D., Grojo D., Charmasson L., Delaporte, P., Uteza, O., Merlen, A., Sanger, A. Torchio, P, 2013 Long range nanostructuring of silicon surfaces by photonic nanojets from microsphere Langmuir films. Journal of Physics D: Applied Physics, 46(14): 145102.

[6] Wang, Zengbo, Guo, Wei, Li, Lin, Luk'yanchuk, Boris, Khan, Ashfaq, Liu, Zhu, Chen, Zaichun, Hong, Minghui, 2011 Optical virtual imaging at 50 nm lateral resolution with a white-light nanoscope. Nature communications 2: 218.

[7] Sylvain Lecler,Yoshitate Takakura, and Patrick Meyrueis 2005 Properties of a three-dimensional photonic jet Optics Lett. 30, 2641-2643

[8] A.V. Itagi and W.A. Challener 2005 Optics of photonic nanojets J. Opt. Soc. Am. A 22, 2847-2858

[9] Seoungjun Lee, Lin Li and Zengbo Wang 2014 Optical resonances in microsphere photonic nanojets J. Opt. 16

[10] Alexis Devilez, Brian Stout, Nicolas Bonod, Evgeny Popav 2008 Spectral analysis of three-dimensional photonic jets Opt. Express, 16, 14200-14212

[11] Cheng-Yang Liu 2013 Photonic nanojet enhancement of dielectric microsylinders with metallic coating J. Optoelecton. and adv. Materials, 15, 150-154

[12] Tingting Wang, Cuifang Kuang, Xiang Hao, and Xu Liu 2011 Subwavelength focusing by microsphere array J. Opt. 13, 035702-035108

[13] S. Lecler, S Haacke, N. Lecong, O. Cr̀egut, J-L. Rehspringer, C. Hirlimann 2007 Photonic jet driven non-linear optics: example of two-photon fluorescence enhancement by dielectric microspheres Opt. Express 15, 4935-4942

[14] Matthias Gerlach, Yury P. Rakovich, and John F. Donegan 2007 Nanojets and directional emission in symmetric photonic molecules Opt. Express, 15, 17343-17350

[15] Patrick Ferrand, Jerome Wenger,Alexis Devilez, Martina Pianta, Brian Stout, Nicolas Bonod, Evgueni Popov, and Herve Rigneault 2008 Direct imaging of photonic nanojets Opt. Express, 16, 6930-6940

[16] S. Yang, A. Taflove and V. Backman 2011 Experimental confirmation at visible light wavelength of the backscattered enhancement phenomenon of the photonic nanojet Opt. Express 19 7084-7093

[17] D. McCloskey, Jing Jing Wang, and J.F. Donegan 2012 Low divergence photonic nanojets fro Si_3N_4 microdisks," Opt. Express, 20, 128-140

[18] A. M. Kapitonov and V.N. Astratov 2007 Observation of nanojet-induced modes with small propagation loss in chains of coupled spherical cavities Opt. Lett. 32, 409-411

[19] D. A. Fletcher, K.E. Goodson, and G.S. Kino 2011 Focusing in microlens close to a wavelength in diameter *Opt. Lett*. 26, 399-40

[20] B. Richards and E. Wolf 1959 Electromagnetic diffraction in optical systems II. Structure of the image field in an aplanatic systems, *Proc. R. Soc. A*, 253(12740 253-258

[21] Daniel McBride and Chin B. Su 2013 Measurement of the depletion beam focal spot using near-field scanning optical microscopy probes *Meas. Sci. Technol*. 24, 12524-12529

[22] Davis, L.W., 1979, Theory of Electromagnetic Beams, Physical Rev. A, 19 (3), 1177-1179.

[23] Devilez, A., Bonod, N., Wenger, J., Gerard,D., Stout,D., Rigneault, H, Popov, E., 2009 Three-dimensional subwavelength confinement of light with dielectric microspheres. *Opt Express*, 17(4): 2089-2094.

[24] Wolf, E., 1959 Electromagnetic Diffraction in Optical Systems. I., An Integral Representation of the Image Field. *Proc. R. Soc. A.* 253 (1274), 349-357.

[25] C.F. Bohren and D.R. Huffman 1998 Absorption and scattering of light by small particles (Wiley, New York).

APPENDIX A

$$M_{o1n}=\cos\phi_p\,\frac{dP_n(y)}{dy}z_n(\rho_p)\hat{e}_\theta-\sin\phi_p[y\frac{dP_n}{dy}-(1-y^2)\frac{d^2P_n}{dy^2}]z_n(\rho_p)\hat{e}_\phi$$

$$N_{e1n}=\cos\phi_p n(n+1)\sqrt{1-y^2}\,\frac{dP_n(y)}{dy}\frac{z_n(\rho_p)}{\rho_p}\hat{e}_r+\cos\phi_p[y\frac{dP_n}{dy}-(1-y^2)\frac{d^2P_n}{dy^2}]\cdot[(n+1)\frac{z_n(\rho_p)}{\rho_p}$$

$$-z_{n+1}(\rho_p)]e'_\theta-\sin\phi_p\,\frac{dP_n(y)}{dy}[(n+1)\frac{z_n(\rho_p)}{\rho_p}-z_{n+1}(\rho_p)]\hat{e}_\phi \tag{49}$$

Here, $y=\cos\theta_p$. According to (A2), (A3) and (A7), B_{o1n} and A_{e1n} can eventually be written as

$$B_{o1n}=\frac{\pi^2\int_0^\infty\int_0^\pi\{-2\sin\theta_p\,\frac{dP_n}{dy}[I_2\cos\theta_p+iI_1\sin\theta_p]-n(n+1)P_n(\cos\theta_p)\sin\theta_p(I_0-I_2)\}d\theta_p d\rho_p}{2\pi\frac{n^2(n+1)^2}{2n+1}\cdot\int_0^\infty j_n^2(\rho_p)\cdot d\rho_p}$$

$$A_{e1n}=\frac{\int_0^\infty\{\frac{j_n(\rho)}{\rho}\cdot N1_n(\rho)-[(n+1)\cdot\frac{j_n(\rho)}{\rho}-j_{n+1}(\rho)]\cdot N2_n(\rho)\}\cdot d\rho}{\pi[n(n+1)]^2(\frac{2}{2n+1})\{(2n+1)(n+1)\int_0^\infty(\frac{j_n(\rho)}{\rho})^2d\rho+\int_0^\infty j_{n+1}^2(\rho)d\rho-2(n+1)\int_0^\infty\frac{j_n(\rho)}{\rho}j_{n+1}(\rho)d\rho\}}$$

$$N1_n(\rho)=\pi^2n(n+1)\cdot\int_0^\pi\{-\sin^3\theta_p\cdot\frac{dP_n}{dy}\cdot(I_0+I_2)+2i\sin\theta_p\cdot\cos\theta_p\cdot\frac{dP_n}{dy}\cdot I_1\}d\theta_p$$

$$N2_n(\rho)=\pi^2\int_0^\pi\{[\sin\theta_p\cos\theta_p\,\frac{dP_n}{dy}-\sin^3\theta_p\,\frac{d^2P_n}{dy^2}][\cos\theta_p(I_0+I_2)+2i\sin\theta_pI_1]+\sin\theta_p\,\frac{dP_n}{dy}(I_0-I_2)\}d\theta_p \tag{50}$$

Where $j_n(\rho)$ is the spherical Bessel function of order n, $P_n(\cos\theta_p)$ is the Legendre function, $y=\cos(\theta_p)$, and I_0 , I_1 , and I_2 are focal functions given in equation (A5)-(A6) with $k_a r_p$ define as ρ . Numerical calculations using the formula given above yield $A_{e1n}=-i\cdot B_{o1n}$ like the plane wave case except that the value of B_{o1n} is different and changes with different degree of focusing.

APPENDIX B

Table 1: Expansion Coefficients E_n in case one

	NA =0.4		NA =0.8	
n	E_n (10^{-3})		E_n (10^{-3})	
	Z_0 = 0	Z_0 = 3.9 um	Z_0 =0	Z_0 = 3.9 um
1	-147.7i	46.906+96i	-0.086-591.3i	125.90+82.09i
2	79.44	-52.88+24.74i	285.28-0.03i	-47.61+67.92i
3	53i	-15.98-36.54i	161.85i	-45.36-35.20i
4	-38.4	27.66-11i	-94.70-0.02i	28.81-32.70i
5	-28.86i	7.702+21.98i	0.03-55.00i	24.24+24.90i
6	22.14	-17.95+5.307i	31.37+0.03i	-22.65+18.31i
7	17.13i	-3.49-14.89i	-0.03+17.54i	-12.99-20.20i
8	-13.3	12.45-2.078i	-9.67-0.03i	18.49-8.86i
9	-10.27i	0.974+10.43i	0.02-5.22i	5.33+16.88i
10	7.9	-8.71+0.115i	2.73+0.02i	-15.21+2.29i
11	6.04i	0.538-7.232i	-0.01+1.34i	0.30-13.42i
12	-4.57	5.94+1.016i	-0.60-0.01i	11.48+2.44i
13	-3.43i	-1.35+4.82i	0.01-0.25i	-4.14+9.43i
14	2.56	-3.83-1.55i	0.12+0.01i	-7.29-5.36i
15	1.88i	1.64-2.98i	-0.01+0.09i	6.08-5.15i
16	-1.37	2.26+1.65i		3.06+6.31i
17	-0.994i	-1.58+1.65i		-6.06+1.14i
18	0.716	-1.143-1.465i		0.54-5.39i
19	0.512i	1.311-0.738i		4.37+1.86i
20	-0.365	0.422+1.137i		-2.75+3.13i
21	-0.259i	-0.953+0.1844i		-1.80-3.17i
22	0.182	-0.0158-0.7712i		3.13-0.52i
23	0.126i	0.601+0.0955i		-0.55+2.70i
24	-0.086	-0.16+0.448i		-1.98-1.33i
25	-0.0566i	-0.136-0.1886i		1.72-1.13i
26	0.035	0.1914-0.2072i		0.31+1.91i
27	0.02i	0.122+0.177i		-1.48+0.42i
28		-0.1515+0.0595i		0.88-0.98i
29		-0.0165-0.1213i		0.40+1.06i
30		0.091+0.0104i		-0.96-0.13i
31		-0.0236+0.0634i		0.49-0.66i
32		-0.0398-0.0276i		0.27+0.64i
33		0.0259-0.0217i		-0.58-0.09i
34		0.0093+0.0207i		0.33-0.37i
35		-0.0142+0.001017i		0.10+0.40i
36		0.00352-0.0079i		-0.31-0.12i
37		0.00261+0.00509i		0.23-0.15i
38				-0.02+0.03i
39				-0.13-0.13i
40				0.15-0.02i
41				-0.07+0.10i
42				-0.02-0.09i

Table 2: Expansion Coefficients E_n in case two

n	E_n (10^{-3})				
	$Z_0 = 0$	$Z_0 = 191$nm	$Z_0 = -191$nm	$Z_0 = 318$nm	$Z_0 = -318$nm
1	-0.005-3275.57i	2159.56+1967.75i	-2159.56+1967.75i	-1576.378+1751.8i	1576.378+1751.8i
2	973.47+0.23i	-786.771+489.505i	-786.771-489.505i	-324.901-140.743i	-324.901+140.743i
3	-0.235+170.534i	58.261-310.84i	-58.261-310.84i	402.408+140.743i	-402.408+140.743i
4	66.789-0.138i	84.267-166.01i	84.267+166.01i	-218.194+152.719i	-218.194-152.719i
5	0.041+62.427i	-96.68-8.202i	96.68-8.202i	-3.73-134.321i	3.73-134.321i
6	-2.53+0.003i	27.256-8.44i	27.256+8.44i	31.7+52.977i	31.7-52.977i
7	-0.015+0.027i	-29.745+15.41i	29.745+15.41i	-44.698-22.378i	44.698-22.378i
8	-17.13-0.035i	-0.167-20.362i	-0.167+20.362i	25.023-12.123i	25.023+12.123i
9	0.035+3.886i	-2.68+6.37i	2.68+6.37i	-11.351+5.716i	11.351+5.716i
10	-12.457+0.0165i	-4.368-12.783i	-4.368+12.783i	7.93-13.949i	7.93+13.949i
11	0.001-5.934i				
12	-3.91+0.002i				
13	0.008-6.68i				
14	2.075+0.016i				
15	-0.0127-3.206i				

Table 3: Expansion Coefficients E_n in case three

n	E_n (10^{-3})		
	$Z_0 = 0$	$Z_0 = -318$nm	$Z_0 = -636$nm
1	-0.005-3275.57i	1576.378+1751.8i	This data will
2	973.47+0.23i	-324.901+140.743i	Come out soon!
3	-0.235+170.534i	-402.408+140.743i	
4	66.789-0.138i	-218.194-152.719i	
5	0.041+62.427i	3.73-134.321i	
6	-2.53+0.003i	31.7-52.977i	
7	-0.015+0.027i	44.698-22.378i	
8	-17.13-0.035i	25.023+12.123i	
9	0.035+3.886i	11.351+5.716i	
10	-12.457+0.0165i	7.93+13.949i	
11	0.001-5.934i		
12	-3.91+0.002i		
13	0.008-6.68i		
14	2.075+0.016i		
15	-0.0127-3.206i		